AN ACCELERATOR BASED *IN VIVO* MEASUREMENT OF ALUMINUM IN HUMAN BONE BY NEUTRON ACTIVATION ANALYSIS

AN ACCELERATOR BASED *IN VIVO* MEASUREMENT OF ALUMINUM IN HUMAN BONE BY NEUTRON ACTIVATION ANALYSIS

By

Ana Pejović-Milić, M.Sc.

A Thesis

Submitted to the School of Graduate Studies

in Partial Fulfillment of the Requirements

for the Degree

Master of Science

McMaster University

MASTER OF SCIENCE (1998) McMaster University

(Medical Physics) Hamilton, Ontario

(Physics)

TITLE: An Accelerator Based *In Vivo* Measurement of Aluminum in Human Bone by Neutron Activation Analysis

AUTHOR: Ana Pejović-Milić, M.Sc. (University of Belgrade)

SUPERVISOR: Professor David R. Chettle

NUMBER OF PAGES: xi, 86.

ABSTRACT

Aluminum is a neurotoxin and has been recognized as a causative agent for dialysis encephalopathy and renal osteodystrophy, as well as possibly being related to Alzheimer's disease. General public exposures to aluminum have increased in the modern, industrial age stimulating scientists to inquire into the degree of risk associated with such widespread use of aluminum.

Aluminum is thought to be stored in bone, therefore, development of an *in vivo* method for the determination of aluminum in human bone, suitable for routine monitoring of patients and population is the goal of this study.

Using neutron activation analysis, low-energy neutrons are produced on the KN accelerator inducing the $^{27}Al(n,\gamma)^{28}Al$ reaction in an irradiated site. Two different shapes (cylindrical and flat) of aluminum doped tissue equivalent phantoms, simulating both bone and soft tissue, have been built. Calibration lines, detection limits and doses delivered with the different shapes of phantom have been discussed, and compared to the previously published results. Two detection systems, an assembly of two large NaI(Tl) detectors and a hyperpure germanium detector, have been compared as well.

The results achieved suggest that this technique may provide an alternative choice to painful bone biopsy for the *in vivo* monitoring of aluminum intoxication from long-term exposure.

ACKNOWLEDGMENTS

My grateful thanks go to my supervisor, Dr. David R. Chettle, who willingly took on the task of leading me into the field of Body Composition, and constantly reviewed this project. David's help and understanding have permitted me to achieve not only a second M.Sc, but inner satisfaction and peace.

Appreciation is also offered to Dr. Fiona E. McNeill for valuable support and advice throughout duration of this work. I would like to thank the members of my committee, Drs. W. V. Prestwich and C. E. Webber for their help during the completion of this project.

Thanks to Jim Stark and Winston Williams for technical assistance and patience during my experiments, and to Rebecca Murphy for fast running (she almost qualified for Nagano 98!).

I extend my gratitude to my colleagues, Joanne O'Meara and Michelle Arnold, for review and translation of this text from my "English" to understandable English language. Also, appreciation goes to the graduate students in medical physics for the open and stimulating scientific environment that I have enjoyed at McMaster.

Last but not least, these years were made tolerable by the understanding and encouragement of my family, Dejan, Mihailo and Luka.

I am grateful to McMaster University for the opportunity and the financial support offered specially to the Eugene G. Bolotkin fund.

TABLE OF CONTENTS

Chapter III Experiment design

Chapter IV Phantoms

LIST OF FIGURES

LIST OF TABLES

Chapter I

Introduction

1.1 *In Vivo* Neutron Activation Analysis

The technique of *in vivo* neutron activation analysis (IVNAA) depends on the excitation of nuclei within the body by an external source of neutrons (Cohn S.H., 1980). Neutrons may be produced using reactors, accelerators or radioisotopes. Although the neutron energies obtained from these sources vary widely, neutrons in the mega and kilo electronvolt range may be used for IVNAA. Also, for measurements at superficial sites thermal neutrons could be used.

Incident neutrons lose energy by elastic and inelastic nuclear scattering and, eventually, become thermalized by the medium, resulting in neutrons with energies in the milli electron volt range. At these energies the neutron capture cross section (σ) is inversely proportional to the neutron velocity for most elements. Following thermal neutron capture, emission of gamma rays may occur either promptly or following the radioactive decay of radionuclei formed by the interaction. Incident neutron interactions

are inelastic neutron scattering {(n,n'γ)}, charge particle emission {(n, α) or (n, p)} and multiple neutron production {(n, 2n)} (Scott M.C., Chettle D.R., 1986).

The excited nucleus will revert to a stable state by the emission of gamma rays of energy specific to that particular isotope. Therefore, the intensity of the gamma emission can be used as a measure of the amount of that isotope, and hence, element in the body if a gamma ray with high probability has been produced. However, the gamma ray emission spectra are usually very complex giving a small yield for the interaction of interest. In addition it is possible to produce the same product by neutron capture reactions with other elements, or the element of interest may interact with neutrons through many different interactions, leading to reduced yield.

Furthermore, the outgoing gamma rays are attenuated exponentially through any tissue between their point of origin and the detector. This, however, is generally not a dramatic effect as the gamma rays produced in neutron activation are typically of sufficient energy that they have fairly long attenuation mean free paths in tissue, and their measured intensity simply falls as $1/r^2$, where r is the distance to the detector.

For maximum gamma ray intensity, one wants to set the detector as close as possible to the target organ and with minimum interfering tissue. The chosen detector should have an efficiency that is independent of the body size and shape, and it should have the best possible energy resolution. The use of different sizes and types of detector may affect the technique sensitivity and an advantage can be achieved by measuring a target organ or parts of the body, where the element is concentrated. Large NaI(Tl)

detectors are normally used, because of their high efficiency, unless the gamma ray spectrum requires the use of a high resolution detector such as that available with germanium semiconductors detectors.

The neutron source should provide uniform neutron delivery throughout the tissue under investigation. Unfortunately, the distribution of thermal neutrons is far from uniform because the distribution of incident neutrons decreases exponentially from the surface and there is the migration of slowed neutrons from the incident site. The other two factors influencing uniform neutron delivery are target organ size and the distribution of the measured element. Uniform neutron distribution can be achieved only for small organs, like kidney, and for elements distributed over a small volume. Nonuniform distribution of neutrons can be a factor limiting measurement accuracy. This problem may be solved if product of the neutron flux and detector's response is achieved to be uniform.

Finally, the magnitude and distribution of the associated radiation dose has to be balanced against the medical value of any *in vivo* measurement. Neutrons indirectly ionize a medium implying some risk to the patient with any IVNAA. Most neutron irradiation involve exposure to gamma rays as well, therefore, this source of radiation must also be considered. A given dose to a subject affects experimental design through the selection of neutron source as well as the required shielding, since reducing the radiation dose to the subjects is essential for adopting IVNAA as routine monitoring in occupational medicine, toxicology or epidemiology. Furthermore, aside from shielding the subject and others performing the measurement from unnecessary dose, it is necessary to shield the detectors

from both interfering cosmic gamma rays and rays produced inside the shield. All this will effect the experimental design in practice, which can make the neutron activation analysis setup inconvenient and bulky.

A wide range of elements has been measured using IVNAA. A review of such applications has been done by several authors (Cohn S.H, 1980; Chettle D.R. and Fremlin J.H., 1984; Scott M.C and Chettle D.R., 1986). Generally, the elements of common interest are hydrogen, oxygen, nitrogen, calcium, sodium, chlorine, cadmium, silicon and phosphorous. Also, there is a wide range of minor reactions that have been investigated for magnesium, potassium, copper, mercury, aluminum, iodine etc.

In short, the success of the technique depends on the abundance and the position in the body of the element to be measured, the probability and the types of neutron reactions which occur with that particular element, and the characteristics of the decay products. The choice of neutron source and irradiation technique is influenced by the depth and extent of the target organ, as well as maximizing sensitivity while minimizing patient dose.

1.1.2 *In Vivo* Neutron Activation Analysis of Aluminum

Aluminum may be measured as either total body aluminum or aluminum in a part of body via the thermal neutron reaction $^{27}Al(n,\gamma)^{28}Al$ (σ = (231±3) mb). ^{28}Al is radioactive, with a half life of 2.25 min., and decays by the emission of a 2.865 MeV β^- particle accompanied by a 1.78 MeV gamma ray (100 %).

In addition to this thermal neutron reaction, aluminum undergoes the fast neutron reactions $^{27}Al(n,p)^{27}Mg$ and $^{27}Al(n,\alpha)^{24}Na$. Each of these three nuclear reactions have an interfering reaction between the neutrons and some other element present in the body. For the $^{27}Al(n,\gamma)^{28}Al$ reaction a further complication is the interference from fast neutron nuclear reactions of $^{31}P(n,\alpha)^{28}Al$ and $^{28}Si(n,p)^{28}Al$, with thresholds of 1.95 MeV and 4 MeV respectively. Since these reactions also produce ^{28}Al, the measured intensity of 1.78 MeV gamma rays will in general be partially due to the presence of ^{31}P and ^{28}Si in the irradiated sample. The $^{27}Al\ (n,p)^{27}Mg$ reaction suffers from the $^{26}Mg(n,\gamma)^{27}Mg$ reaction, while the $^{27}Al(n,\alpha)^{24}Na$ from the $^{23}Na(n,\gamma)^{24}Na$ reaction.

For the (n,p) and (n,α) reactions with ^{27}Al the interference is caused by thermal neutrons, thus a moderation of fast and slow neutrons within the body will always provide some thermal flux to provoke these interfering reactions. Opposite to that, the $^{27}Al(n,\gamma)^{28}Al$ reaction is a thermal reaction itself interfered by the fast neutron reactions. Therefore, it gives possibility to eliminate the fast neutron component from the neutron beam preventing the activation of ^{31}P and ^{28}Si.

After exposure to a neutron beam and transfer time, the sample counting is usually done with low-background detectors, usually NaI (Tl) detectors with large surface areas, as previously discussed. The area or amplitude of the ^{28}Al peak, at 1.78 MeV, gives a measure of the quantity of aluminum present in the body once all necessary corrections are made.

The main target organs affected by aluminum toxicity are the bone, the brain, the liver and the kidneys. During aluminum exposure, urinary aluminum elimination was on average seven times higher than that of a control group, but it remained high up over a prolonged period suggesting a tissue loading (Moreno A. et al, 1994). The storage organ for aluminum is thought to be bone mineral, and possibly liver and kidneys. The brain presents an inconvenient site for a diagnostic procedure. Also, liver and kidney contain many other toxic elements and are enclosed with other tissue which makes aluminum measurement difficult. Therefore to measure aluminum quantity, bone is an appropriate site, since it is both the target and the storage organ with thin overlying tissue.

According to the chemical composition of Reference Man cited by ICRP 23 (1975), the content of aluminum in the skeleton is 21 mg. Knowing that 1.5 % of the skeleton is in one hand (the typical irradiated site during the procedure), the expected content of aluminum in the hand of a healthy adult is 0.3 - 0.4 mg. Bond in the hand is composed of 95 % of cortical and 5 % of trabecular bone (ICRP 70, 1994). For successful IVNAA of aluminum, where only part of the body is exposed to a neutron beam, it is assumed that aluminum is homogeneously distributed in the skeleton. Due to the small amount of overlying tissue between the external neutron source and the bone mineral in the hand, the attenuation of neutrons by tissue is considered to be negligible.

The absolute amount of aluminum in the hand depends upon the size of the hand and overlying tissue as well as the irradiation and counting geometry. However, it was shown that need for extensive corrections for all these factors can be eliminated through

the use of γ rays emitted by ^{49}Ca as a normalization parameter for the ^{28}Al intensity detected. It was demonstrated as well that Al/Ca ratio is simply proportional to the aluminum concentration in bone (Ellis K.J. et al., 1988).

Calcium neutron activation is based on the $^{48}Ca(n,\gamma)^{49}Ca$ (σ_{TH} = (1.09±0.14)b) reaction. The amplitude of the ^{49}Ca gamma peak positioned at 3.084 MeV (100%), gives a measure of the quantity of calcium present in the bone. In the Reference Man skeleton there is 1180 g of natural calcium or 18 g in one hand. Therefore, 2.125 g of ^{48}Ca may be expected in the skeleton and 32 mg in the hand, knowing that ^{48}Ca comprises 0.187 % of natural calcium.

1.2 Why Is Aluminum Important?

Being the most abundant element in the earth's crust, aluminum is naturally in our surroundings. The increased presence of aluminum in surface waters close to aluminum plants is reported in North America, Norway and Russia. This is generally linked with sulfur dioxide emissions from smelters resulting in acid rainfall. As a result, the pH factor of some lakes and brooks are lowered, and aluminum is released from acidified terrestrial soil and lake sedimentation. Flood and melted snow may lower the pH of ground water, and therefore, cause an increase of aluminum release into lakes and streams. Also, in the areas where plants' waste have been discharged there is higher concentration of ionic

aluminum forms in the surrounding environment. Aluminum surface water pollution results in the accumulation of the metal in fish organs, which therefore leads to aluminum accumulation in human food (Rodushkin I., 1995).

Beside aluminum intake through polluted water, aluminum is present in drinking water, added as aluminum sulfate, a coagulant in the treatment of water. Further, daily intake of aluminum depends on diet. The reported aluminum concentration in tomatoes is 2.2 mg/kg, beans 6.6 mg/kg, cooked beef 6 mg/kg, chocolate is over 13.2 mg/kg and chewing gum 0.5 mg per stick (Nicar M.J., 1992). Moreover, aluminum phosphates are fillers in baking powder and processed cheeses, aluminum sulfate is used in pickling and aluminum calcium silicate is added to table salt to help it run freely.

With the use of aluminum pots, pans and foil, some aluminum leaches into food, especially with acidic foods. Cooking with fluoridated water in aluminum cookware increases the aluminum in the water and the food. Still, the amounts we obtain in this manner are small compared with those from additives and drugs. Aluminum hydroxide is used as a phosphorus binder and antacid, and dialysis patients ingest 100 mg/kg body weight per day. Or, aspirin prescribed for rheumatoid arthritis may add 700 mg per day (Nicar M. J., 1992). A average daily intake of aluminum in food and fluids is estimated as 45 mg (ICRP 23, 1975).

Beside general public exposure, a number of recently growing industries result in potential aluminum exposure due to one's occupation. There is significant risk of occupational exposure to aluminum, such as in the airplane or automobile industry, and

smelters. There is evidence for systematic aluminum absorption from occupational exposure to airborne aluminum. Occupational exposure to aluminum has been associated with increase in both urinary aluminum excretion and serum aluminum. The bone mineral content, which was determined in the lumbar spine by means of dual photon absorptiometry, showed no significant difference between exposed and non-exposed workers to aluminum powders. The bone density values in the exposed subjects was 1.00 g/cm^2 compared to 1.02 g/cm^2 in control group (Schmid K. et al, 1995). This work might imply that in healthy individuals, with normal kidney function, there is no evidence of significant change in bone density caused by aluminum deposition in skeleton.

Another example of occupational exposure is found between 1944 and 1979, miners in northern Ontario were exposed to a finely ground powder of aluminum (McIntyre Powder) to prevent silicon lung disease. The powder was 15 % elemental aluminum and 85 % aluminum oxide. Miners inhaled it for 10 minutes before each underground shift. These miners have no neurological disorders but have an overall poorer performance on cognitive tests compared with a reference group (Rifat S. L., 1990). Unfortunately, aluminum burden in bone has not been measured in this group.

Aluminum is probably the least toxic metal, although the concern is that it has become so widely used that it is now found in higher levels in human tissue. In fact, aluminum toxicity has only recently been discovered, and it appears to be more toxic with pre-existing reduced kidney function. With the main source of aluminum intake being ingestion, the overall health risks associated with aluminum exposure are strongly

dependent on the degree of absorption. This in turn is largely dependent by the chemical form of aluminum ingested. For instance, some forms of aluminum such as aluminum hydroxide, are poorly absorbed from the gastrointestinal tract, whereas organic compounds of aluminum such as aluminum citrate, pass very rapidly from the food into the blood. Furthermore, absorption can be catalyzed or inhibited by the presence or absence of other compounds. On the other hand, aluminum itself may reduce the absorption of selenium and phosphorus from the gastrointestinal tract and thereby result in an adverse health effect indirectly (Nicar M. J., 1992). Overall, aluminum has a low absorption in the gastrointestinal tract, which naturally protects the body against its neurotoxic effects.

It is not clear how aluminum functions or interferes with activities in the human body, although it has been suggested the aluminum interferes with some magnesium functions. It may reduce vitamin levels or bind to DNA, and it has been correlated with weakened tissue of the gastrointestinal tract.

Whatever the mechanism, acute aluminum poisoning has been associated with constipation, colicky pain, anorexia, nausea, skin problems, and a lack of energy. Slower and longer-term increase in aluminum body burden may cause muscle twitching, numbness, paralysis, and fatty degeneration of the liver and kidney. Skin rashes may occur with local irritation from aluminum anti perspirants as well. However, toxic levels of aluminum are as yet unknown.

Only ten years ago many illnesses were linked to the presence of aluminum in the body. More recently published articles have more concentrated on chronic renal failure (Dahl E. et al, 1990), dialysis osteomalacia (Dahl E. et al, 1990; Worth D.P. et al, 1989), dialysis encephalopathy (Dahl E. et al, 1990; Crapper D.R. et al, 1980), anemia (Dahl E. et al, 1990), and Alzheimer's disease (McLachlan D.R.C. et al, 1991; Crapper D.R. et al, 1980; O'Mahony D. et al, 1995) as the main diseases caused by aluminum poisoning.

Accumulation of aluminum in patients with chronic renal failure has been attributed to the use of aluminum-based phosphate antacids and to the contamination of dialysate water. The hemodialysis fluid based on drinking water brings aluminum directly into the blood stream. In these patients the tissue accumulation of aluminum causes an osteomalacia, renal osteodystrophy or encephalopathy. The first two illnesses are types of bone deformations, the loss of bone matrix, due to the deposition of aluminum during skeletal repair. In bone, aluminum impairs skeletal mineralization and diminishes bone cell activity, producing cross links between collagen fibrils. The normal range of quantitative bone aluminum content in the over-60 age group has not been established yet, but for a younger healthy group it ranges from 0 to 20 μg/g dry weight (O'Mahony D. et al, 1995). Aluminum induced bone disease is now less frequent due to the use of water purification for dialysate solution and the substitution of calcium salts for aluminum containing antacids to bind phosphate.

As well as the debilitating bone structure, bone aluminum accumulation can also impair red blood cell production. This effect is similar to anemia, however it is a form that

is resistant to iron supplementation. A further adverse health effect observed in dialysis patients that has been linked to aluminum is dialysis encephalopathy. This is a form of dementia, and it is this possible link between aluminum and mental deterioration that has become the main focus of researchers concerned about aluminum exposure.

Aluminum toxicity has been implicated in aging brain disorders. Alzheimer's disease and Parkinsonism have both become more frequent and this may be correlated with an increase in aluminum toxicity. In Alzheimer's disease increased aluminum levels in the brain tissue have been absorbed, in the form of aluminum alkaloid, and an increase in what are called "neurofibrillary tangles" which tend to reduce nerve synapses. There also appeared to be a weakening of the blood-brain barrier in Alzheimer's disease, and this may allow a variety of brain toxins to reach the central nervous system.

A recently published study has tested the hypotheses about the connection of stored aluminum and Alzheimer's disease. In this study trabecular bone aluminum content was measured in patients with diagnosed senile dementia of the Alzheimer type. Quantitative analysis done by atomic absorption spectrometry showed lower aluminum content (11.9±4.04 μg/g dry bone) in the patients than in the control group (18.2±7.37 μg/g dry bone) (O'Mahony D. et al, 1995). These results imply that aluminum content in trabecular bone may not influence the disease. On the other hand, it has been suggested that there is an increasing portion of circulating, unbound aluminum in blood which may cross the blood brain barrier causing brain damage, and thus may originate from bone. Some previous studies have found a higher aluminum content in trabecular bone than in

cortical (Alfrey A.C. et al, 1976; Lefebvre A. et al, 1988), supporting the measurement of aluminum in trabecular bone, and further, the attempt to correlate it with the incidence of the diseases.

Another study has implicated aluminum as a toxic environmental factor of considerable importance. A survey of eighty-eight country districts in England and Wales pointed out a relationship between the risk of Alzheimer disease and the aluminum concentration present in drinking water over the previous decade. This study has shown that the risk of Alzheimer's disease in people under the age of 70 years is 1.5 times greater in districts where the mean aluminum concentration in drinking water exceeds 11 μg/l than in districts where the concentration is less than 1 μg/l (Martyn C.N., 1989). A similar study was performed in Newfoundland in the area of Bonavista Bay where a significant excess of deaths could not be explained by differences in sex, ethnic origin, family origin or morbidity patterns. The area was reported to have a high aluminum concentration in drinking water, that is 165 μg/l. Furthermore, two epidemiological studies in Norway showed the risk of death from senile dementia in a region with a high concentration of aluminum in water (200 μg/l) is 1.48 times higher than in a region with a low aluminum concentration (20 μg/l) (McLachlan D.R.C. et al, 1991). However, the link between Alzheimer's disease and aluminum is still controversial and presents an open field for extensive scientific work.

All this has caused an increasing number of scientists to inquire into the degree of risk associated with such widespread use of aluminum.

Knowing more about aluminum and its effect on humans, but still far from understanding all aspects the following recommendations (McLachlan D.R.C. et al, 1991) have been made that still wait to be presented to public:

- Human exposure to aluminum should be limited. Current evidence supports the hypothesis that a major reduction in the ingestion of aluminum would reduce the incidence of Alzheimer's disease.
- A goal for the daily intake of aluminum from all sources should be 3 mg or less.
- Municipal processed water should be regulated so that the aluminum concentration is less than 50 μg/l.
- The aluminum content should be listed on the packages of all substances marked for human use and ingestion including food, water, cosmetics, toothpaste and pharmaceutical products.

These conclusions present a vigorous "anti-aluminum" view, and therefore might be opposed or challenged by a "pro-aluminum" way of thinking.

Aluminum toxicity is currently diagnosed through a qualitative method, namely the histochemical analysis of a bone biopsy sample taken from the iliac crest. The invasive procedure is often painful and consequently has a low patient acceptance. Because of this and the awareness of the potential increase in harmful effects due to aluminum poisoning, a few research centers in the world have tried to develop a new, non-invasive technique to measure aluminum status using *in vivo* neutron activation analysis.

1.3 Performance of Different Methods for *InVivo* Measurement of Aluminum

The noninvasive *in vivo* measurement of aluminum body burden based on neutron activation analysis of ^{27}Al in bones is presented as a feasible and practical technique of monitoring aluminum levels in the body. Previous studies have been undertaken at Brookhaven National laboratory, Long Island, New York (Ellis K.J. et al., 1988) and at McMaster University, Hamilton (Palerme S. et al, 1993) using reactor based sources, at Swansea (Wyatt R.M. et al., 1993) using a ^{252}Cf source and at the University of Birmingham using a Dynamitron accelerator to produce neutrons via the $^{3}H(p,n)^{3}He$ reaction (Green S. et al, 1993).

The overall performances of these different methods for *in vivo* aluminum measurements are summarized in table 1.1.

At all four research centers, neutron activation analysis of aluminum in the hand was performed. Each center used the neutron sources mentioned above, delivering different equivalent doses to the hand, with different detection limits and sensitivities.

As seen in table 1.1, the Brookhaven study, using a nuclear reactor as the neutron source, demonstrated a low detection limit and, as well as a low delivered dose. The pilot study at the McMaster reactor demonstrated that the interference reactions arising from the interaction of fast neutrons with phosphorus and silicon in the hand, reduces the effectiveness of reactor based neutron source. Also, a nuclear reactor is a questionable

neutron source for routine diagnostic procedure simply in terms of availability to the medical community.

Place	Source	Hand dose (mSv)	Effective dose* (μSv)	MDL (mg)	MDL x √ hand dose
Brookhaven	Nuclear reactor	< 20	26	0.4	1.8
Swansea	Moderated ^{252}Cf (2.2 MeV)	36	47	2.2	13.2
Birmingham	^{3}H(^{1}H,n)^{3}He;	50	65	2.0	14.1
Birmingham	E_p = 1.2MeV	20	26	1.8	8.0
		20	22**		
McMaster	Nuclear reactor	43	56	2.8	18.4

* Assuming that 1.5 % of total body skeleton and skin is in one hand, and that 0.1 % of the hand dose will be delivered to the rest of the body;
** (Green et al, 1993) ; the assumptions were that the hand and lower forearm compose approximately 3% of the total skin and skeleton, and that the patient's body receives 0.05 % of hand dose;

Table 1.1: Performance of different methods for *in vivo* measurement of aluminum in bone.

The ^{252}Cf neutron source has low neutron flux (2 x 10^5 n/cm^2 s) and interference from the fast neutron reaction with ^{31}P. A cyclic activation analysis can increase the amount of activation of aluminum (240 s of irradiation in five cycles overall), but the detection limit is still much higher than the value of aluminum in the Reference Man hand due to the low neutron flux. The advantage of this source is that it is inexpensive compared with the other proposed neutron sources, and is portable.

The final proposed neutron source, an accelerator-based source, can produce neutrons with a maximum energy below the threshold for interfering reactions and with adequate flux for hand measurements as shown by studies at the University of Birmingham and McMaster University. A further benefit of this source is that it could in principle be

transported (mobile accelerator). This suggests an accelerator may be the best source for IVNAA currently available.

The effective dose for different protocols for *in vivo* measurements of aluminum in bone has been calculated, and results are also included in table 1.1. For comparison, table 1.2 presents the effective doses arising from a range of diagnostic examinations (Rainbow A., 1995). The average value of natural background radiation in Canada and dose limits set by the Atomic Energy Control Board (AECB) are also included. Comparing these values with the calculated effective doses to the hand due to a single IVNAA aluminum measurement (range 22 - 65 μSv), it may be concluded that the delivered dose is at an acceptable level, comparable with a chest radiograph and below other standard diagnostic procedures. Also, it should be noted that one aluminum IVNAA measurement will deliver approximately 4 % of the average value of natural background radiation in Canada from all sources, and is far below the upper limit of AECB recommendations. And furthermore, the AECB dose limit for a hand of an occupational exposed worker is 750 mSv per year.

Procedure	Typical Effective dose (μSv)
Chest radiograph	20 -50
Thoracic spine radiograph	900
Pelvic/abdominal radiograph	1300
Average PET scan	3900
Barium examination	3800 -7700
Body CT Scan	6000 - 16000
Head CT scan	2000
Natural background, all sources	2000
AECB occupational dose limit per year	50000
AECB Member of the Public per year	5000

Table 1.2. Effective dose for a range of diagnostic examinations. Average value for natural background in Canada and dose limits set by the Atomic Energy Control Board (AECB) are also included.

The delivered dose is small but we may estimate the risk to the patient from a single *in vivo* bone aluminum measurement if we assume a linear dose/risk relationship. The nominal probability coefficient for stochastic effects (fatal cancer) for the whole population is given as 5×10^{-2} per Sv. The corresponding value for severe hereditary (genetic) effects is given as 1.3×10^{-2} per Sv (Rainbow A., 1995). Therefore, for the range of calculated effective doses (22 - 65 μSv, table 1) the risk of fatal cancer to the whole population due to a single IVNAA hand aluminum examination is between 1×10^{-6} and 3×10^{-6}. The risk of severe hereditary effects to the whole population is from 3×10^{-7} to 8×10^{-7} for this same dose range.

Adhering to the radiological principle of ALARA (as low as reasonably achievable) further reduction of the absorbed dose can be achieved by additional shielding. However, the effective dose and the risk delivered during a single *in vivo* neutron activation analysis of aluminum in bone is at acceptable level within current criteria for the whole population.

Therefore, it is proposed that the use of an accelerator based neutron activation system for the direct *in vivo* monitoring of bone aluminum values in patients, may provide an alternative choice to painful bone biopsy for the detection of aluminum from long-term exposure.

1.4 Previous McMaster Study of Aluminum in Humans

This thesis is largely a continuation of the Pilot Studies for In Vivo Bone Aluminum Measurement by Stephanie Palerme performed at McMaster University in 1993 (Palerme S., 1993).

The first part of pilot study was the selection of the best neutron source available at the present time at McMaster University. Two neutron beam ports at the McMaster Nuclear Reactor as well as the use of the KN accelerator were investigated. For aluminum measurements in bone, high thermal neutron flux is desired to minimize the phosphorous interference and to maximize the activation per unit time. The fast neutron flux was calculated to be 1.1 % and 40 % of the thermal flux for the two reactor ports, while the KN accelerator beam showed no component of the fast neutrons at all.

At the time of the pilot study, the KN accelerator was inaccessible for experiments and, therefore, further aluminum measurements were done on the better neutron port, where the higher thermal flux was measured. Further experiments were done to set experimental procedure and data analysis.

The next step of this early study was to construct the physiological simulation of phantoms of a Reference Man hand, with varying amounts of added aluminum. After switching from a solution to a fixed, cylindrical phantom, a calibration curve and minimum detectable limit for the system was calculated (see table 1.1).

The main goal of the pilot study was to investigate the feasibility of the routine aluminum measurement in bone with the available neutron sources at McMaster University. For more details, please, refer to Palerme S., 1993 work.

This work presents a step forward in developing a routine aluminum procedure in humans bone, continuing from this earlier pilot study in terms of optimizing the neutron source, irradiation procedure and initial phantom design in order to improve system sensitivity while minimizing subject dose.

Chapter II

Characteristics of Neutron source, Moderator and Cavity

2.1 Neutron Energy

Prior to exposing the aluminum doped phantoms to the neutron beam we have characterized our neutron source, a KN-accelerator, in which the production of neutrons is based on the $^{7}Li(p,n)^{7}Be$ reaction. This endothermic nuclear reaction with a Q of 1.64 MeV can produce neutrons with energies of few keV and up. The threshold energy E_{th}, based on the conservation of momentum is

$$E_{th} \geq \left(\frac{M_{Li} + m_p}{M_{Li}}\right) \cdot |Q|$$

Thus, the minimum proton energy necessary for the reaction is 1.88 MeV. The neutron energy is a strong function of both angle and proton bombarding energy. The energy distribution of the neutrons was measured using a ^{3}He proportional counter for various angles of deflection from the incident beam direction at constant proton energy.

The ^{3}He noble gas is used as a detection medium for neutrons through the $^{3}He(n,p)^{3}H$ (σ_{th} = 5330 b) reaction. This reaction induced by slow neutrons has a Q value of 764 keV which leads to opposite directed reaction products with energies of 573 and

191 keV for the proton and the triton, respectively, if one assumes the neutron has essentially no kinetic energy upon interacting. The triton and proton are emitted in opposite directions to each other because the incoming neutron carries no appreciable momentum.

In a large size detector, all the initial kinetic energy of the neutron may be deposited in the form of kinetic energy of the triton and proton. Since the range of these products may not be small compared with the dimensions of the counter, the wall effect may appear in middle or small size detectors. If this is the case, a step structure on the left side of the full energy peak (at 764 keV) with small peaks corresponding to the triton (at 191 keV) and proton (at 573 keV) energies may be seen in the acquired spectra, see figure 2.1.

The spectrometer was connected to high voltage (3000 V), pulser and amplifier. The amplified signal is then simultaneously monitored with an oscilloscope while sent to a personal computer (IBM 386 computer with Aptec 6.31) passing through an analog-to-digital converter and multichannel analyzer (MCA), which are part of a MCA Aptec card, before being displayed spectrally on the monitor.

In this experiment the ^{3}He spectrometer was placed (20±4) cm from the ^{7}Li target for various angles of deflection from the incident beam direction, and (175±4) cm from the floor. The beam direction is denoted with 0 degree angle. Some angles have been omitted due to the presence of other equipment in the target room. The detector was placed on foam to eliminate the "microphone effect" registered as periodic oscillation on the

oscilloscope screen.

These experiments were performed using protons of (2.25±0.02) MeV energy and 2 μA current on the target with an irradiation time of 3000s. These settings, regarding the proton energy, are identical to those used in the aluminum measurement. A typical neutron spectrum emitted by the KN - accelerator, in beam direction, as measured by the ^{3}He detector is shown in figure 2.1.

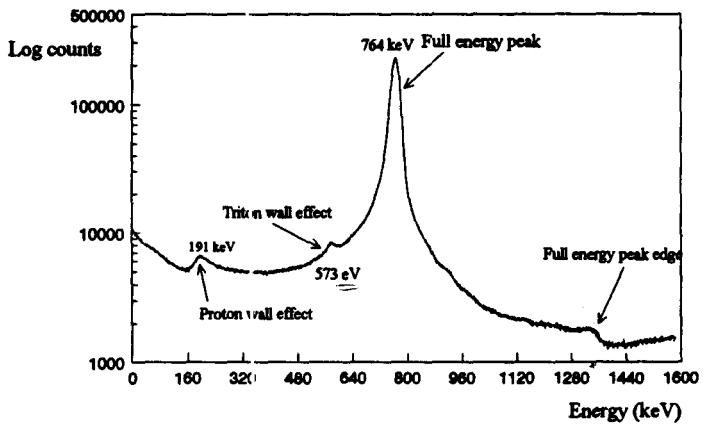

Figure 2.1 Spectrum of thermal neutrons emitted by the beam at 0 degree acquired by the ^{3}He detector.

. The spectrum demonstrates the presence of all the expected features of a neutron spectrum acquired with a ^{3}He counter. The main peak corresponds to neutrons of low energy compared to 764 keV interacting with ^{3}He to create a 191 keV triton and 574 keV proton. The full energy peak edge above this main peak in the energy spectrum corresponds to the maximum energy released in the ^{3}He(n,p)^{3}H reaction. This is, of course, comprised of the Q value as well as any initial kinetic energy of the neutron and/or the ^{3}He atom involved in the event. As any residual kinetic energy of ^{3}He in the detector is a fixed value for a particular set of physical conditions, the energy difference between the

main peak and its high energy edge is dictated by the maximum kinetic energy of the neutrons incident on the detector.

The change in position of the edge in the spectrum can be used to determine the change in the maximum kinetic energy of the neutrons incident on the detector for different angles. Therefore, it was necessary to assume that the maximum kinetic energy in beam is that predicted by theory for the ^{7}Li (p,n)^{7}Be reaction with (2.25±0.02) MeV protons. Then the maximum neutron energy off beam at various positions was determined by the shift in the edge from its position in beam.

Figure 2.2 shows the experimentally measured maximum neutron energy calculated in absolute terms assuming this value at 0 degree. This figure also demonstrates the theoretical prediction of maximum neutron energy off the beam for a different angle θ that is based on the equation

$$E_n^{1/2} = \frac{1}{m_{Be} + m_n}\left\{\cos\theta(m_p m_n E_p)^{1/2} \pm \left\{m_p m_n E_p \cos^2\theta + (m_p + m_n)[m_{Be}Q + (m_{Be} - m_p)E_a\right\}^{1/2}\right\}$$

where E_i is the energy of incident proton or emitted neutron, and

m_i is proton, neutron or beryllium mass.

According to this calculation, protons of (2.25±0.02) MeV energy on the target will produce a maximum energy of 520 keV along the beam axis ($\theta = 0^0$).

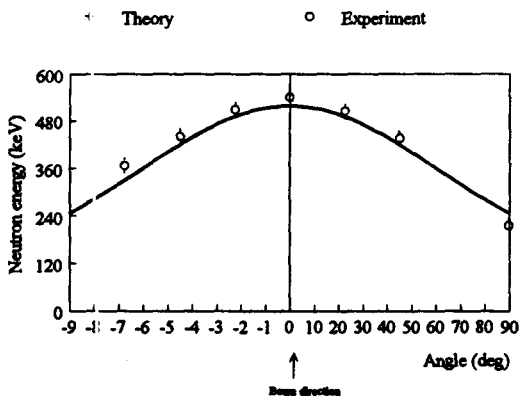

Figure 2.2 Neutron energy for various angles of deflection from the beam.

As expected, the neutron energy distribution is symmetrical around the neutron beam and the shape of the experimental data corresponds well with theoretical prediction. The neutron energy spectrum may be easily varied by changing the bombarding proton energy. The kinetics of the ^{7}Li (p,n)^{7}Be reaction dictate the linear increase in maximum neutron energy with proton energy (Yanch J.C. et al, 1992). On the other hand, the decrease in maximum neutron energy is accompanied with a decrease in yield. Another way of changing the neutron energy is by varying the target thickness. The resulting neutron spectrum is the superposition of a series of thin targets yields with successively decreasing incident proton energy. Thus, having a single thin Li-target would result in more monochromatic neutron spectrum.

It should be noted at this point that the maximum neutron energy in beam is a significant feature of this system. This maximum value of 520 keV is such that the interference reactions of fast neutrons with phosphorous and silicon are not energetically permitted. This is a critical feature of the system in terms of dramatically simplifying the analysis of the aluminum measurement spectra. This emphasizes the advantage of the KN accelerator for measuring aluminum in human bone.

2.2 Flux of Thermal Neutrons

The thermal neutron flux within a possible irradiation cavity was measured using an ^{115}In foil (1 x 1 cm) via the thermal neutron reaction $^{115}In(n,\gamma)^{116}In$ (figure 2.3). The indium samples were very thin foils (1 x 1 cm) made from an indium wire (95.7 % ^{115}In and 4.3 % ^{113}In). $^{116m2}In$ with a short half life decays during the transfer time of 30 s, but the $^{116m1}In$ spectra (half life of 54.1 min) were successfully acquired for 30 min. There are a number of γ rays emitted by the $^{116m1}In$ isotope, and the peaks with the greatest intensity being 1.293 (85 %), 1.097 (55.7 %), 0.818 (11.6 %) and 0.416 MeV (32.4 %). The area of the 1.293 MeV peak, originated from de-excitation from the first exited to ground level, was used for further data analysis because of its large intensity.

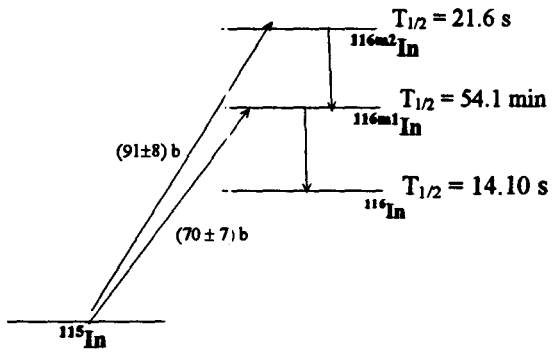

$^{115}In(n,\gamma)^{116}In$

Cross section = (161 ± 11) b

Figure 2.3 Indium neutron activation reactions.

The foils were protected by Scotch tape which was also used to place them in different positions in the polyethylene sheets (average thickness 12.6 mm), to measure the

change of neutron flux, and further, to investigate the best cavity design. The irradiation time was varied, depending of a distance from the target and degree of attenuation by polyethylene, in order to ensure good counting statistics, i.e. maximum of 1 to 2 % uncertainty. The foil measurements were also repeated using a different incident proton energy on the target.

The activity of the indium foils was measured with a pure Ge detector (Ge Ortec, model GMX - 25190 - S), placing the foils in the center of the detector's surface, and acquiring spectral data with a PC computer. After correcting for the irradiation, transfer and counting time as well as the detector efficiency, the foil activity was obtained. The activity measured in the foils was assumed to be only due to the thermal neutrons. A few neutrons in the beam will have the indium specific resonance energies, but for this study no correction was made for the possible resonance activation.

To investigate the desirable thickness of polyethylene between the neutron beam and the phantom/hand, the indium foils were aligned with the neutron beam axis and activated, changing the number of polyethylene sheets between the source and the foil. The results are presented in figure 2.4, showing the same trends with incident protons energies between 2.00 and 2.25 MeV. The highest thermal flux was achieved with 2.5 cm of polyethylene with a proton beam of 2.25 MeV. The distance from the ^{7}Li target was 42 cm. Based on these results, all further experiments were performed using (2.25±0.02) MeV protons.

The next set of foil activation was done to investigate the influence of neutron

backscattering from polyethylene, placed behind the phantom/hand, to maximize the thermal flux inside the future irradiation cavity. With 2.5 cm polyethylene between the target and indium foil, centered on the beam axis, the foil activation was measured setting different numbers of sheets behind the foil on axis. The saturation thickness of (2.0±0.5) cm was achieved with one to two sheets of polyethylene.

Ideally a uniform distribution of thermal flux is desired, the spatial variation of thermal flux was measured with 2.5 cm of polyethylene between the beam and foils and the saturation thickness behind, at 2.5 cm and 42 cm from the ^{7}Li target. The average thermal flux density inside the cavity was $(3.3\pm0.2)10^{6}$ and $(1.2\pm0.2)10^{5}$ $n/cm^2/s$ respectively.

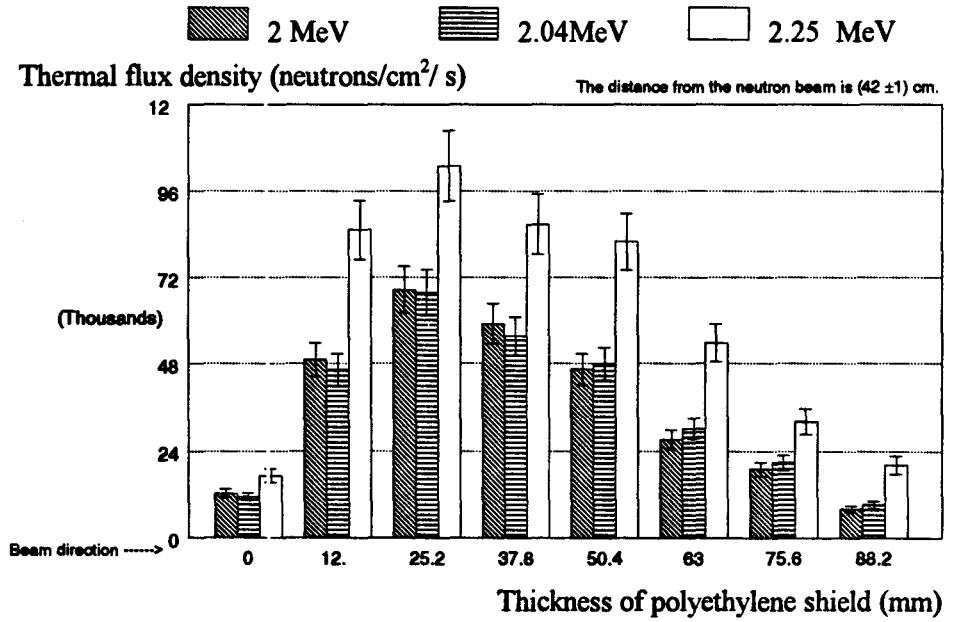

Figure 2.4 Relative change in thermal neutron flux density with different thickness of polyethylene shields between the beam and the indium foil.

For all foil measurements since a small and thin foil is used the probability of an interaction is small for any specific neutrons. Further more, assumption is made that the thermal flux does not vary during the exposure time, meaning that foil activation measurements cannot provide information about any time variation of the neutron flux during the exposure.

These flux measurements allow us to estimate only the thermal dose delivered to the hand during a three minute irradiation would be 6 and 0.2 mSv for two distances, using the fluence to dose equivalent conversion factor from ICRP 21 (1971). Assuming that 1.5 % of total body skeleton and skin is in one hand, and that 0.1 % of the hand dose will be delivered to the rest of the body, the effective dose to the patient would be 0.78 μSv at 2.5 cm, and 0.026 μSv at 42 cm.

2.3 Cavity Design

Polyethylene -(CH_2)n- is rich with hydrogen atoms, therefore, it has a high scattering cross section for neutrons, and is, therefore, a good neutron moderator. On the other hand, polyethylene has a large neutron absorption coefficient, and beside thermalizing neutrons it also absorbs them, decreasing the number of neutrons in the beam. At the present time, the irradiation cavity has been made only from polyethylene. The reason for this was the immediate availability of polyethylene shields in the lab, its low

price, and light and convenient cavity design.

The variation in the neutron flux with different thickness of polyethylene pre-moderator indicated that the highest thermal flux was achieved with two shields on each side of the indium foil (see Sec 2.2). Regarding the top and one side wall, the assumption was made that they will effect the flux in the same way as the back wall, therefore, they were added to the cavity. However, one side of the cavity has to be open to insert the phantom or the patient's hand inside the irradiation cavity.

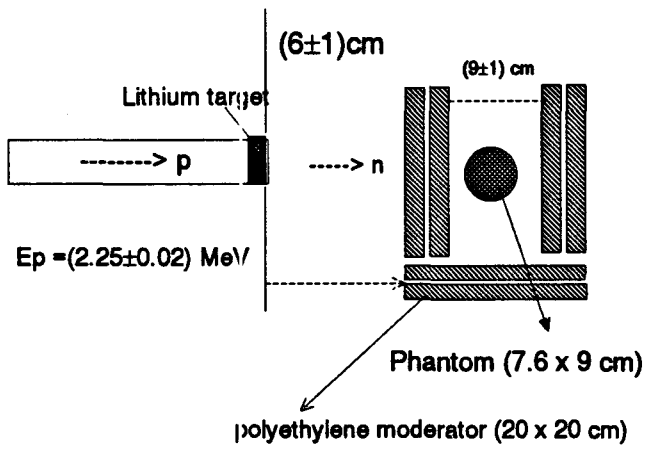

Figure 2.5 Cavity and experiment design.

As a result of the flux measurements previously presented, a simple irradiation cavity was built with each wall made of polyethylene sheets (2 x 12.6 mm thick). The cavity "gap" may be set to different sizes which was designed to accommodate two sizes of measured phantoms in this experiment. The polyethylene irradiation cavity within the context of the overall experimental design is presented in figure 2.5.

Chapter III

Experimental design

3.1 Experimental design

The experimental set up and procedure have been further developed based on the results presented in the Pilot Studies For *In Vivo* Bone Aluminum Measurements by Stephanie Palerme as previously mentioned. The KN - accelerator has been used as the neutron source throughout these experiments, as it had been recommended. See section 1.3 for factors affecting the choice of the neutron source and a discussion of the strengths and weaknesses of the available sources.

Different cavity designs, made from polyethylene, have been studied by measuring the flux of thermal neutrons and the optimal configuration has been established (see Sec. 2.3). The space inside the cavity was designed to fit two different sizes and shapes of investigated phantoms.

In this work two detection systems have been investigated to find the more suitable one. First, two NaI (Tl) detectors with large cross sectional area were used to measure aluminum in the set of phantoms placed in quasi-4π geometry. The second detection system utilized one HPGe detector. The signals from all detectors were acquired by

commercial software, and the data were further analyzed (see Sec. 3.3).

The irradiation procedure timing protocol was constant throughout the experiment independent of which phantoms or detectors were used. The irradiation time of the phantoms was 180 s, followed by a transfer time of usually 20 - 30 s and a counting time of 300 s.

The irradiation time was chosen based on findings in the pilot study (S. Palerme, 1993). The measured neutron flux (Sec 2.1) was considered sufficient to activate aluminum present in the phantoms within the 180 s irradiation time. An increase in the neutron flux may be achieved by shortening the distance from the beam or by increasing the current. Both factors can affect the irradiation time as well as a dose delivered to the phantom. Therefore, their effects have been studied further.

The distance between the target room and the room housing the shielded detectors has dictated the transfer time to be between 20 s and 30 s. At the beginning of the experiments two NaI (Tl) detectors were placed in the same room with the neutron beam, shielded by a concrete wall. This shield as well as the lead shield around the detectors was insufficient to protect them from neutron activation reactions. The detectors were activated via the $^{23}Na(n,\gamma)^{24}Na$ and $^{127}I(n,\gamma)^{128}I$ reactions, and the emitted γ rays interfered with the phantom spectra acquired. Therefore, the detectors were moved to a room separated by a heavy, steel door far from the neutron beam (approximate 60 m), thereby substantially increasing the transfer time but greatly reducing counting rate from sources other that the activated sample.

Governed by the half-life of ^{28}Al (2.25 minutes) the counting time was 5 minutes. Two half-life times were enough to maximize the signal over the background counts.

The positioning of phantoms was done manually placing them in the center of the irradiation cavity (see Fig. 2.5, Sec 2.3).

The initial set of experiments was performed at (42±2) cm from the Li - target. The cavity was placed on a mobile cart of adjustable height. Before each set of irradiation, the height ((177±3) cm) and distance were checked to ensure the cavity was centered on the beam line. Inside the cavity, the phantoms have been placed at 8.5 cm height from the cavity bottom.

For further experiments, the distance was set at (6±1) or (2.5±0.5) cm from the target. At that time a fixed shelf was built to minimize the distance between the irradiation cavity and the neutron source to increase the neutron flux, and to fix the positioning of the cavity from the floor. For this experimental setup, the distance was checked before each set of measurements.

During all measurements a dose monitor, Snoopy, was positioned at 67.5 degree on the right side of the beam at a distance of 2 m. The Snoopy measurements were used to monitor the field in the target room during irradiation, which is a part of routine safety procedure. While running the accelerator with 2.25 MeV incident proton energy on the Li-target, the field ranged from 5.5 to 14 mSv/h depending on the cavity distance from the target.

3.2 Detection systems

3.2.1 NaI(Tl) detector

The photon counting system was based on two large NaI(Tl) detectors facing each other (200 mm x 50 mm thick), built in a Pb-shield environment (figure 3.1), and arranged to achieve 4π-geometry. The air gap between detectors for the initial, cylindrical set of phantoms was 9 cm. After flatter phantoms were built, the air gap was made smaller, and set at 4.5 cm. Both gaps were sufficient to accommodate a patient's hand for future *in vivo* measurement.

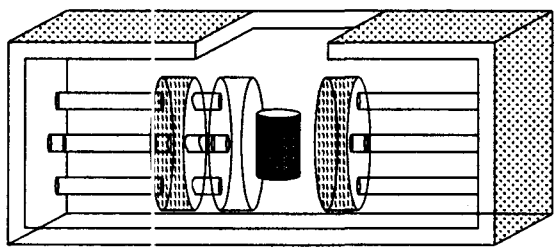

Figure 3.1 NaI(Tl) detection system.

The scintillation crystal has four photomultiplier tubes connected in parallel in each detector. Detectors are independently connected to preamplifiers (CI model 1405, serial number: 128231 and 48175), and then to amplifiers (Harshaw, models: Na-23 and Na-32). From both amplifiers, the signals are summed (Ortec, model 43388) and sent to a personal computer, where spectra were acquired and saved by commercial software Aptec 6.31.

The detection system is shielded with 3 cm of lead on each side, and during the phantom

measurement a lid was closed. The shield has decreased significantly a background by protecting the detectors from cosmic rays.

Before each series of spectra, the gain of both detectors was adjusted such that the gains are matched. This test was done by monitoring a 1.27 MeV ^{22}Na peak with each detector separately, and then the detectors summed signal. To keep the gains similar from experiment to experiment the 1.27 MeV peak was set at a standard position of (538±5) channels. If a gain shift was observed throughout one set of experiments, that was adjusted by the computer analysis of spectra.

It should be noted at this point that this detection system is arranged in a quasi-4π geometry thus minimizing a loss of γ-rays. Furthermore, this geometry allows γ-rays that have undergone Compton scattering in one detector, to be detected by the other detector, if the scattered γ-ray and the released electron are counted simultaneously. Placing detectors closer, which was accomplished by making flatter phantoms, produced an almost 4π-geometry, and an increase in system's efficiency was noticed further lowering the detection limit.

Figure 3.2 presents typical spectra acquired by this detection system set at the 9 and 4.5 cm gap. The spectra of flat phantoms have a ^{24}Na summed peak at 4.1 MeV, which had not been seen before, providing supporting evidence that detection efficiency have been improved just by lowering the distance between the detectors.

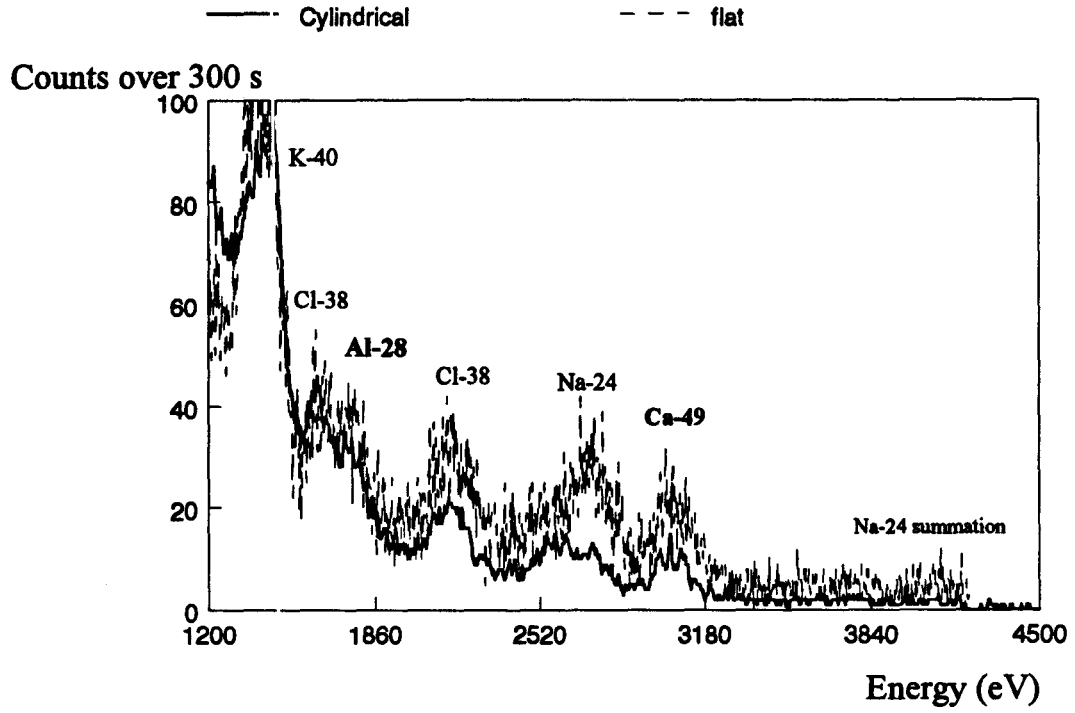

Figure 3.2 Typical spectra of cylindrical and flat phantoms acquired by two large NaI(Tl) detectors arranged in quasi 4π-geometry.

3.2.2 HPGe Detector

Some preliminary experiments with a single hyperpure germanium detector were done. One NaI(Tl) detector was replaced with the HPGe detector (Ge Ortec, model GMX-25190-s), in the above mentioned detection circuit. Cylindrical phantoms were placed to come into contact with the detector's surface, covering it completely. The flat set of phantoms has not been measured with HPGe detector because their surface was too big compared with the detector's, and aluminum peak height was insignificant over a room background.

HPGe detector has better resolution the NaI(Tl) detector, but NaI(Tl) detector

has superior efficiency over HPGe detector. HPGe better resolution has led to well separated aluminum and chlorine peaks, and therefore, simplified the fitting technique. Nevertheless, the fitting of clearly defined aluminum peak with Marquardt method did not improve the uncertainty on the peak height. Thus, even superior HPGe resolution has not improved the minimum detectable limit (for more details refer to Sec. 5.1 and 5.2).

3.3 Spectral Analysis

3.3.1 Analysis of Spectra Acquired using NaI(Tl) Detectors

Data analysis has been done using the non-linear least-squares optimization method first developed by Marquardt (Bevington P.R., 1992), and separate fits are applied to the aluminum and calcium characteristic peaks. Summed spectra from two NaI (Tl) detectors were analyzed.

The poor energy resolution of the NaI (Tl) detectors governed the choice of the fit equations. Ultimately it was determined that a single exponential to fit the background with a gaussian to fit the aluminum peak was the beast approach. The following seven parameter equation was used in analyzing the aluminum peak area for all NaI(Tl) spectra acquired

$$y(x) = A(1)\cdot\exp(A(2)\cdot x) + A(5)\cdot\exp\left[-\left(\frac{x-A(4)}{A(3)}\right)^2\right] + A(6)\cdot\exp\left[-\left(\frac{x-A(7)}{A(3)}\right)^2\right] \quad (1)$$

where A(1) is the amplitude of the background,

A(2) is the exponent of the background,

A(3) is the aluminum peak width,

A(4) is the position of the aluminum peak,

A(5) is the amplitude of the aluminum peak,

A(6) is the amplitude of the chlorine peak,

A(7) is the position of the chlorine peak.

The independent and dependent variables, x and y, have been used in the same manner throughout this section, where x corresponds to the channel number in the spectrum while y is the number of counts in the channel.

The chlorine peak in the spectrum arises from thermal neutron activation of chlorine present in both the phantoms and a subject's hand. This process results in a γ ray that is close in energy (140 keV) to the ^{28}Al γ ray, and the acquired spectrum has the aluminum peak positioned in the higher energy tail of the chlorine peak (see figure 3.2). Therefore, a gaussian for the chlorine peak was included in the aluminum fitting routine.

In all spectra, the background was well modeled by a single exponential, and this could be explained by the response of the detector. The use of gaussian to model the peaks produced by NaI(Tl) spectra has been studied previously and is broadly used model.

After it had been checked that this fit worked, it was decided to reduce the number of parameters by fixing the width of gaussian. An inverse variance weighted mean of the widths given by the analysis of the cylindrical phantom spectra was used for the fixed value for all subsequent analysis.

In an attempt to reduce the number of parameters and improve further the fitting technique, it was decided to link the chlorine peak position with the aluminum peak position. It would have been difficult to float aluminum and chlorine positions and widths independently, and the assumption was thought to be justifiable over this energy range. After the chlorine peak was linked to the aluminum peak only the aluminum position was floated and the fitting equation became

$$y(x) = A(1)\cdot\exp(A(2)\cdot x) + A(4)\cdot\exp\left[-\left(\frac{x-A(3)}{w}\right)^2\right] + A(5)\cdot\exp\left[-\left(\frac{x-(A(3)-53.5)}{w}\right)^2\right] \qquad (2)$$

where A(1) is the amplitude of the background,

A(2) is the exponent of the background,

A(3) is the position of the aluminum peak (Cl linked to Al),

A(4) is the amplitude of the aluminum peak,

A(5) is the amplitude of the chlorine peak,

w is the aluminum peak width.

To get a better fit and to increase the degrees of freedom of the model it is necessary to fit over the maximum possible number of channels. Also, other spectral features appearing at higher and lower energies than the characteristic peak would require

modeling, thereby potentially increasing the number of fitting parameters. Therefore, as many channels were fit as possible around the characteristic peak such that no other spectral features were included (with the exception of the chlorine peak which is too close in energy to the aluminum peak to exclude).

Since the absolute amount of aluminum in the hand depends upon the size of the hand as well as the irradiation and counting geometry, the ratio of the aluminum to calcium signals are taken to derive the aluminum concentration in hand (see Sec. 1.1.2). Therefore, a similar Marquardt method was necessary for fitting the calcium peak in the appropriate region of the spectrum.

As with the aluminum region, it was decided that the width could be fixed in order to reduce the number of fitting parameters. Again, the inverse variance weighted mean value from the phantom spectra was used, and the final equation selected for fitting the calcium peak is then given as

$$y(x) = A(1)\cdot\exp(A(2)\cdot x) + A(3)\cdot\exp\left[-\left(\frac{x - A(4)}{w}\right)^2\right] \qquad (3)$$

where A(1) is the amplitude of the background,

A(2) is the exponent of the background,

A(3) is the amplitude of the calcium peak,

A(4) is the position of the calcium peak.

w is the calcium peak width.

3.3.2 Analysis of Spectra Acquired using HPGe Detector

A Marquardt method was used to analyze the data acquired with the HPGe detector as well. Improved energy resolution allows the aluminum peak to be fit independently of the chlorine peak, since they are well separated, typically by (136±3) channels. Therefore, the final term of the equation (1) is unnecessary thereby reducing the number of parameters. As with the NaI(Tl) spectra, the peaks are modeled with gaussians, however, the improved resolution implies the numerical values of the widths have changed. The background shape also changed with the switch in detectors and the best fit was empirically determined to be a straight line. Therefore, the initial fitting function for the HPGe spectra is given as

$$y(x) = A(1)\cdot x + A(2) + A(5)\cdot \exp\left[-\left(\frac{x - A(4)}{A(3)}\right)^2\right] + A(6)\cdot A(5) \qquad (4)$$

where A(1) is the gradient of the background,

A(2) is the intercept of the background,

A(3) is the peak width,

A(4) is the position of peak,

A(5) is the amplitude of peak,

A(6) is the step height.

The linear behavior of the background is governed by the response of HPGe detector in the monitored energy range. The characteristic peaks obtained by germanium detectors are asymmetrical, therefore, the step function was introduced by the last term of the previous fitting equation. The term A(6) x A(5) is only present for x < A(4), otherwise there is no step. At the present time, the gaussian function to model the characteristic peak was felt to be a justifiable fitting approach for the purpose of this experiment.

Since the modeling of the chlorine peak has been eliminated, this one function was used to fit both the aluminum and calcium regions of the spectra independently. An inverse variance weighted mean was taken giving the width of the aluminum or calcium peak separately. Thus, the fitting equation with a reduced number of parameters could be used for further analysis, given as

$$y(x) = A(1)\cdot x + A(2) + A(5)\cdot \exp\left[-\left(\frac{x - A(4)}{w}\right)^2\right] + A(3)\cdot A(5) \qquad (5)$$

where A(1) is the gradient of the background,

A(2) is the intercept of the background,

A(3) is the step height,

A(4) is the position of peak,

A(5) is the amplitude of peak,

w is the width Al or Ca peak.

3.3.3 Further Data Analysis

The amplitude of the aluminum and calcium peaks calculated by the Marquardt method were further analyzed. These amplitudes were corrected for transfer, irradiating and counting times separately, due to the differences in their half-lives. The calibration lines were then obtained by plotting the ratio of these corrected amplitudes (Al/Ca) versus the aluminum mass in each phantom, and then determining the regression line by a linear least-squares method For each set of measurements, such as data obtained with the different phantom designs or detection system, the Minimum Detectable Limit (MDL) was estimated.

Minimum Detectable Limit is defined as twice the precision at a zero concentration measurement divided by the slope of the calibration line. This is a common definition of lower limit of detection, set as the concentration that gives rises to a signal intensity that is twice the standard deviation of the measured intensity in the limit of low aluminum concentration. As the concentration goes to zero, the peak intensity goes to zero and, therefore, the uncertainty in the peak intensity is determined by the uncertainty in the background counts under the peak.

Therefore, the MDL is proportional to $\sqrt{}$(background) / calibration slope. Since the slope is the peak intensity over the concentration, the MDL proportionally related to this variable as

$$MDL \propto \frac{\sqrt{N_B}}{N_P} \cdot concentration \tag{6}$$

or

$$MDL \propto \frac{\sqrt{R_B \cdot t}}{R_p \cdot t} \cdot concentration \tag{7}$$

or

$$MDL \propto \sqrt{\frac{R_B}{t}} \cdot \frac{concentration}{R_P} \tag{8}$$

where R_P and R_B are the peak and background count rates.

For fixed R_B and the calibration line slope, the MDL is proportional to $1/\sqrt{t}$, i.e. longer measurement time provides a smaller lower limit of detection. However, dose due to the subject is proportional to the measurement time for a given neutron source. Comparing systems based on the MDL alone may be misleading in that an improved detection limit may be at the cost of higher dose to the patient. Therefore, system comparisons should be based on both the MDL and the patient dose (see table 1.1, Sec. 1.3).

3.4 Dose

A dose delivered to the patient's hand during routine aluminum measurement is made up of the energy deposition of different types of radiation such as neutrons, gamma rays, recoil and decay of some atoms.

A neutron dose depends on the incident neutron energy, since the radiation weighting factor for neutrons also depends on its energy. Reactions induced in the hand by the thermal neutrons are $^{1}H(n,\gamma)^{2}H$, $^{14}N(n,p)^{14}C$, $^{35}Cl(n,\gamma)^{36}Cl$, and $^{23}Na(n,\gamma)^{24}Na$.

The dominant damaging effect is done by the neutron activation of nitrogen atom. There are three processes provoked by this reaction, such as the production of protons, recoil and decay of the ^{14}C atoms, thus contributing to the thermal dose at different levels. On the other hand, the dose delivered by the gamma rays from the reactions with hydrogen, chlorine and sodium is not significant, because the hand has thin layer of soft tissue and rather small and thin bones, meaning that almost all gammas will escape from it before making energy deposition. Also, gamma rays have the smallest radiation weighting factor of 1. The dose from the decay of carbon and sodium atoms is negligible compared with the dose deposited by the protons. It may be noted that the dose from thermal neutrons comes from a mixture of the low (γ) and high LET (p, ^{14}C recoil) types of radiation.

3.4.1 Dosimeter

A dose measurement, at present, was done with the Anderson and Braun neutron remmeter (Tracerlab, Model NP-1 portable monitor). The monitor, colloquially called Snoopy, consists of a unique polyethylene moderator / attenuator assembly, BF_3 detector, and associated electronics used to convert the detector pulse output to a meter reading and recorder / scaler signal. The scaler output is useful if integrated dose information rather than dose rate is desired, as in this experiment, and if accurate measurements at very low count rates are required.

The incident neutrons with energy greater than thermal are moderated by elastic scattering in the polyethylene cylinder. After the neutrons are thermalized, they are counted by a BF_3 proportional counter via the $^{10}B(n,\alpha)^7Li$ reaction. The Snoopy has high sensitivity and accuracy at low dose rates, plus manufacturers claim excellent stability from thermal energy up to 10 MeV.

But the neutron monitor is not nearly as accurate as often assumed. There are problems with a mixed field response as well as with monitor's positioning. In practice these problems are not so critical in the sense that they together may cause less than a 50 % over response (Rogers D.W., 1979). The non-isotropic response of cylindrical monitor means that they could underestimate the dose equivalent of a mono-directional neutron field by a factor of two if they were not rotated in order to find the maximum reading (Rogers D.W., 1979).

The instrumental setup for a dose measurement used the monitor's negative 1 V scalar output connected to the signal input of Timer / Scaler unit (Baird - Atomic Scaler, model 955-150). The counting time was governed by the timer to achieve low uncertainty on the acquired number of counts.

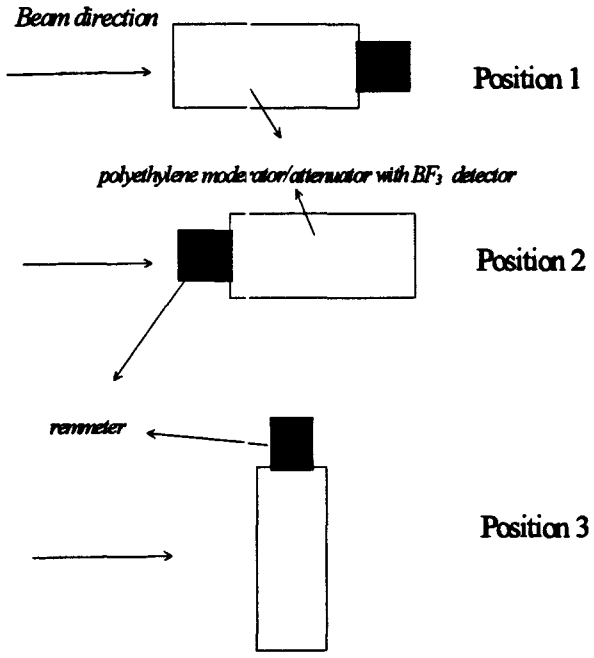

Figure 3.3 Positioning of Snoopy for dose measurement.

3.4.2 Dose Dependence on Dosimeter Rotation

Before measuring a dose for routine aluminum procedure, the Snoopy was rotated to find its maximum reading as recommended. Depending where the incident neutrons hit the monitor surface, see figure 3.3, the dose was measured for three different positions of the Snoopy (each denoted by a number). This was measured at (2±1) and (42±1) cm from the target to the surface of monitor, aligned with the beam, because these distances present two extremes for the phantom measurements.

As expected, the observed dose depends on the Snoopy rotation. One point arising

Distance (cm)	Position	Dose (mSv)
2.5	1	6.109±0.005
	2	5.918±0.005
	3	6.115±0.005
42	1	4.181±0.005
	2	3.276±0.005
	3	4.497±0.005

Table 3.1 Dose dependence on the Snoopy rotation

from table 3.1 is that the highest dose was observed when a Snoopy is placed in the position #3. Therefore, to eliminate underestimation of a dose all measurements have to be done in the position #3.

Second point to be drawn from same data is that the dose depends less on the monitor rotation when approaching the Li-target. The measured doses range from 0.97 to 0.99, and from 0.73 to 0.93 relative to the highest observed dose at 2 and 42 cm, respectively. When the Snoopy is placed close to the target it may be concluded that all neutrons deposit energy into it almost independently of position. On the other hand, the dose is more affected by monitor's rotation farther from the target implying that some neutrons pass monitor's surface without interaction. This difference in response has been influenced by the rapid neutron beam divergence from the target.

The dose measured by the Snoopy assumes that the radiation is evenly distributed over its surface meaning that the Snoopy is in an isotropic neutron field. Since Snoopy's cross sectional area is different from the mono-directional beam's cross sectional area, the dose equivalent measured must be corrected by their squared ratio. The beam diameter may be estimated as a 50 % height at full width of the flux peak at required distance. This is a common way to correct a dose measurement done by the Anderson and Braun neutron remmeter to avoid underestimation.

In this experiment, the aluminum activation is performed inside a polyethylene irradiation cavity. Therefore, the spatial variation of thermal flux was measured with indium foils inside the cavity at 42 cm from the target (Sec. 2.2). Since an uniform spatial distribution is noticed, it was impossible to estimate accurately the beam diameter, and further, to correct the dose on a common way.

Based of these observation during each routine aluminum procedure the Snoopy was placed at, so called, standard position at 2 m and 67.5 degree from the Li-target in position #3, to continually monitor the neutron field inside the target room. Regarding the dose delivered during the routine procedure, another Snoopy was placed inside the irradiation cavity aligned with the beam, and the dose was measured relative to the dosimeter at the standard position. Before this dose measurement, the monitor's sensitivity was checked.

3.4.3 Dosimeter's Sensitivity

The sensitivity of dosimeter (9000 counts/mrem) permits the conversion of the counting rate to a dose equivalent rate independently of neutron energy.

The two monitors used have been calibrated every six months, since their purchase, but only their meter readings oriented in position #1. Also, the 1V negative output hardly has been in use whatsoever, and there was no proper documentation for such calibration. Thus, a meter or rate reading was compared with a dose equivalent rate

in a known radiation field.

The Snoopy, usually placed in standard position during aluminum measurements, was placed in known radiation field and meter reading was noticed. Then it was replaced with second monitor, used for a procedure dose measurement.

The first monitor's test was done in the radiation field of ^{238}Pu-Be source with a mean energy 3.5 MeV and the maximum energy 10 MeV. A disagreement was noticed between the two dose readings at 2 cm from the ^{238}Pu -Be source, implying that the Snoopy's sensitivity might have been changed. Thus, the sensitivity was recalculated as (7850±30) counts/mrem for the high energy neutrons emitted from the source, relative to meter reading.

Similar test was done in a neutron field produced by KN accelerator. Again a disagreement was noticed, and the sensitivity was calculated as (4900±50) counts/mrem for neutrons emitted from the Li-target.

The monitor's sensitivity that was estimated in KN-accelerator field is two times smaller than the sensitivity suggested in the manual. Therefore, the dose measurements presented further in this work are corrected with the sensitivity relative to the Snoopy in standard position instead of with the suggested one. One may rather overestimate the dose until an accurate microdosimetry measurement can be introduced.

3.4.4 Dose Measurement

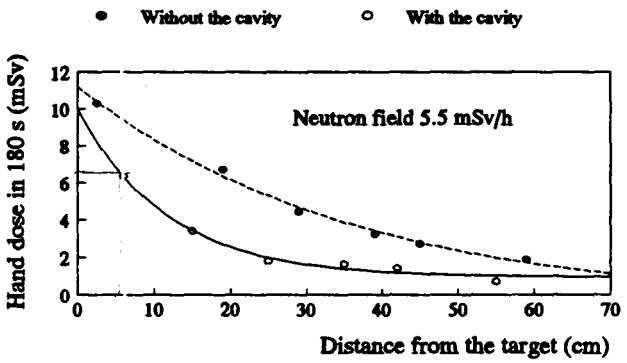

Figure 3.4. Change of hand dose with distance

During a development of procedure for aluminum measurement in bone, phantoms have been irradiated at different distances from the target, neutron field and/or proton energy. To comprise all possible differences in irradiation procedure, and, still, to be able to estimate quickly delivered dose to the phantoms, dose measurements were comprehensive.

In the constant neutron field of 5.5 mSv/h at the standard position of Snoopy, the hand dose decreases as distance increases (figure 3.4). Measurements were done with (°) and without (•) the irradiation cavity while dosimeter was aligned with the beam. Results have demonstrated that the hand dose inside the cavity was 1.6 to 2.5 times smaller than the dose delivered without the cavity depending on distance. This emphasizes another important role that irradiation cavity has in this procedure, beside to increase the flux of thermal neutrons (Sec.2.2). Namely, the dose delivered to a treated patient is reduced to about one half. One of the goals for a prospective medical procedure is to deliver as low

as reasonably possible dose to a patient, and, it has been partially achieved with the polyethylene cavity.

Distance (cm)	Hand Dose correlation to dose at standard position*
2.5	Hand Dose = (7.05±0.22) + (0.35±0.04) Dose; $r^2 = 0.95$
6	Hand Dose = (1.9±0.4) + (0.76±0.08) Dose; $r^2 = 0.94$
42	Hand Dose = (0.17±0.02) + (0.163±0.001) Dose; $r^2 = 0.99$

* Standard Snoopy position at 2m and 67.5 degree from the Li-target

Table 3.2 Hand dose correlation to the dose at standard position.

Further, to investigate the dose dependence on a neutron field inside the target room, one monitor was placed at the standard position and second one aligned with the beam. It was observed that the hand dose linearly increases with the increase of neutron field (table 3.2). It should be underlined, that these dose relations are obtained between two Anderson and Braun neutron remmeters, and that they will change with the change of monitors or their position.

Proton energy (MeV)	Hand dose (mSv)
2.25	6.34±0.07
2.20	6.36±0.06
2.15	7.70±0.08
2.10	7.54±0.08

Table 3.3 Dose dependence on proton energy

With same experiment settings, the dose dependence on proton energy was measured at 6 cm with the dosimeter placed inside the irradiation cavity. Results show no significant change in the delivered dose with the increase of incident proton energy (table 3.3). This might suggest that neutrons with higher energy imposed by the increase of proton's energy are readily thermalized by the irradiation cavity.

A proton current is another parameter that might effect the dose, and KN accelerator is licensed to run up to 30 μA at present time. Also, the thickness of Li-target

will affect the neutron flux, and further the dose. To minimize these effects on the hand dose, the neutron field was monitored rather that the proton current due to instability of current readings. As explained previously, this was done by placing the dosimeter at the standard position throughout all aluminum measurements.

3.4.5 Hand Dose

The advantage of the procedure for aluminum measurement, with KN accelerator and polyethylene irradiation cavity, is the reduction of fast neutron component from the beam. This, besides eliminating interfering reactions on ^{31}P and ^{28}Si, lowers the dose to the patient by factor 1.6 to 2.5. The predominant component in the neutron beam are thermal neutrons, with radiation weighting factor equal 5, compared with the fast neutrons and their radiation weighting factor of 20. This, clearly, lowers the radiation damage to the irradiated tissue while it is inside the cavity.

The dose delivered during one routine aluminum procedure of 180 s, measured with the Anderson and Braun neutron remmeter, is presented in table 3.4. This hand dose is considered as an upper limit on the actual dose due to the irradiation. The whole body dose associated with the hand dose may be estimated in a

Distance (cm)	Dose at Standard Position (mSv/.h)	Hand dose (mSv)	Effective dose (μSv)
42	14	2	2.6
6	5.5	6	7.8
2.5	5.5	9	11.7

Table 3.4 Hand dose delivered during the routine aluminum procedure of 180 s

similar fashion as in Section 1.3.

One must note that a microdosimetry measurement has to be done in the near future. A more rigorous dosimetry will eliminate the fact that the Snoopy detector uses an average quality factor to convert the dose reading to a dose equivalent rate as well as it will consider other sources of radiation present during the procedure.

Chapter IV

Phantoms

4.1 Initial Set of Phantoms

According to the chemical composition of Reference Man cited by ICRP 23, cylindrical aluminum doped phantoms were constructed to simulate both soft tissue and bone during a pilot study of feasibility of aluminum IVNAA at McMaster University (S. Palerme, 1993). Polyester resin was used as a substrate, to which fixed amounts of bone ash (37.53 g), NaCl (2.35 g), Na_2CO_3 (1.33 g) and varying amounts of $Al(NO_3)_3 \cdot 9H_2O$ were introduced. The phantom set consisted of six phantoms corresponding to 0, 0.5, 2, 5, 20 and 50 mg of aluminum. An additional two phantoms, consisting of the resin matrix only and resin with bone ash, were included in this set, to investigate the presence of aluminum in these two components, since resin and bone ash were not of high purity. The aluminum impurity was calculated to be approximately 9 mg per phantom, and has been taken into account throughout all calculations based on this set of phantoms (S. Palerme, 1993).

The above mentioned compounds were added such that the phantoms contained the appropriate amount of only those elements that undergo nuclear reactions with thermal

neutrons having significant spectral features. All other components of soft tissue and bone as given by ICRP 23 were considered inert. For example, hydrogen and nitrogen may react with thermal neutrons emitting prompt γ rays, but these are not detectable with the detection system used. Hydrogen may also undergo elastic scattering with a thermal neutron, however, this will only have an effect on the thermal neutron flux. Oxygen and carbon have low neutron absorption cross sections, and therefore, they are also not considered significant elements to account for with phantom simulations.

As previously mentioned, fast neutrons also produce the interfering reactions such as $^{31}P(n,\gamma)^{28}Al$ and $^{28}Si(n,p)^{28}Al$, with thresholds of 1.95 MeV and 4 MeV respectively. Based on the neutron spectra measurements, the KN accelerator may produce neutrons up to 520 keV with the incident proton energy of 2.25 MeV (See Sec. 2.1) which, therefore, do not have sufficient energy to activate phosphorus and silicon present in the hand. Because of this, these interfering reactions have not been considered during our study, and phosphorus and silicon were not added to the phantoms.

The cylindrical shape, 76 mm diameter x 90 mm height, was chosen to simulate a clenched fist. These dimensions are toward the upper limit of the typical range of the fist size in a normal adult population and, therefore, allows for the conservative design of irradiation facilities.

These cylindrical phantoms were inherited from a previous aluminum study and, because of that, provided an initial set of phantoms with which to test the neutron source.

For a more detailed procedure of the cylindrical phantom construction, please refer to the Pilot Studies For *In Vivo* Bone Aluminum Measurements by Stephanie Palerme.

4.2 Next Generation of Phantoms

To investigate different phantom shapes, a second set of flat phantoms (rectangular, of dimensions 23 x 13 x 2.5 cm) simulating an open hand, doped with low concentrations of aluminum, were made, with the same procedure as the cylindrical ones, to investigate the possibility of improving the system design and lowering the detection limit. This phantom shape is expected to have a lower screening effect during the irradiation, providing better activation of aluminum, as well as allowing the NaI(Tl) detectors to be positioned closer thereby improving detection efficiency.

Preliminary data indicated the new phantom shape may lower the detection limit. However, before building a complete set of flat phantoms it was decided that the source of aluminum impurity in the phantom materials, as previously discussed, should be identified and eliminated, rather that assuming a fixed value and correcting the data accordingly.

4.3 Trace Elements - Mass Spectrometry Analysis

The quantification of trace elements in the chemicals which were used or were being considered for use in constructing the phantoms was investigated by mass spectrometry (Perkin Elmer Sciex Elan 250 ICP-MS) at the geology department at McMaster University.

Bone ash and resin were analyzed because they are not compounds with high chemical purity and they were used for building the cylindrical set of phantoms. As an alternative to bone ash, calcium phosphate may be added in the new set of phantoms to simulate bone present in the hand. Therefore, calcium phosphate was analyzed as well, even though it is a chemical compound with rather high purity.

Semi quantitative analysis of bone ash, resin and calcium phosphate estimated the content of aluminum and calcium in these samples. Then the samples were analyzed by a standard addition method for further accuracy.

The estimated quantity of aluminum was found to be 11 ppm in calcium phosphate and 409 ppm in bone ash. Also, calcium phosphate was found to contain less of other trace contamination than bone ash such as sodium, magnesium and strontium. After these preliminary results, further analyses were done only with calcium phosphate and resin.

The standard addition method is a quantitative method based on the linear increase

of signal due to the known increase in concentration of element present in a solution plus the original unknown concentration of the investigated element.

Three aliquots of the aluminum stock solution were prepared. One aliquot was measured by weight and diluted to a weight that is in the range of the expected aluminum content (X) approximated by the semi quantitative analysis, and lying in the linear range of the instrument (between 1 and 800 ppb). The two remaining aliquots of the stock solution were each spiked with an amount of a standard solution, so that the first spiking would result in a signal of 2 x X, and the second in a signal of 4 x X. The amount of aluminum added by spiking is known, and the total weight of each solution and stock solution is also known. Data analysis may be done either graphically or by regression, and in any event, it should give a linear increase in the signal with each addition of the stock solution. The x intercept gives the value of aluminum present in the sample, and this may be back calculated to the concentration in the original sample.

Tables 4.1 and 4.2 present the measured content of aluminum in resin, calcium phosphate and bone ash, as well as, the estimated quantities of aluminum in the initial, cylindrical and new, flat phantoms.

Initial, cylindrical phantoms	mass in phantom (g)	Al* (ppm)	Al as a tracer in phantom (mg)
Bone ash	37.53	409	15.35
Resin	600	0.192	0.12
	Al as a trace element in cylindrical phantom (mg)		**15.47**

* measured by mass spectrometry

Table 4.1 Al as a trace element in the initial, cylindrical set of phantoms.

New, flat phantoms	mass in phantom (g)	Al* (ppm)	Al as a tracer in phantom (mg)
Calcium phosphate	37.53	47	1.76
Resin	600	0.192	0.10
	Al as a trace element in new phantom (mg)		**1.87**

* measured by mass spectrometry

Table 4.2 Prediction of Al as a trace element in the new, flat set of phantoms.

From the mass spectrometry results, aluminum as a tracer in the initial, cylindrical set of phantoms is present with 15.47 mg of aluminum per phantom (table 4.1). This result is of the same order of magnitude as the aluminum content calculated in the previous pilot study at McMaster University (9 mg per phantom) (S. Palerme, 1993). The main source of this aluminum contamination is bone ash, with some contribution from the resin, as expected.

Calcium content was also analyzed in same way. Accurate assessment of phantom calcium content is critical since all aluminum measurements are normalized to calcium measurement in the phantom/hand. Table 4.3 summarizes the results from these measurements. It was assumed that the only possible source of calcium contamination in the phantom is the resin matrix.

	mass in phantom (g)	Ca* (ppm)	Ca as a tracer in phantom (mg)
Resin	600	27	16.2
	Ca as a trace element in the phantom (mg)		**16.2**

* measured by mass spectrometry

Table 4.3 Calcium as a trace element in the phantoms.

Calcium contamination from resin is 16.2 mg. There appear to be a significant amount of calcium in the resin, the soft tissue phantom material. However, because the level of contamination is constant for all phantoms and there is no attempt to simulate the geometry of bone material and soft tissue of the hand, this will not affect the minimum detectable limit of the system. The calcium contamination in the resin will, simply, result in a slightly larger fraction of total mass arising from calcium in the phantom compared with Reference Man hand. The normalization procedure is, therefore, expected to eliminate any effect arising from the calcium content of the resin.

Regarding the aluminum content in the new, flat set of phantoms aluminum content will approach 1.87 mg, mainly arising from calcium phosphate (~ 94 %). This is a rather unexpected result as the analyzed calcium phosphate is a high purity compound.

These results show that it is extremely difficult to eliminate the presence of aluminum as a trace element in the new set of phantoms, but the use of calcium phosphate instead of bone ash will significantly reduce the contamination.

4.4 New Set of Phantoms

The new, flat set of phantoms (rectangular, of dimensions 23 x 13 x 2.5 cm) were made using same procedure as for the cylindrical ones. Instead of bone ash, $Ca_{10}(PO_4)_6(OH)_2$ (37.53 g) was used to simulate bone in the hand, since it was measured to have lower content of aluminum as a tracer than bone ash. Resin was used as matrix to which all other compound were added to build physiological simulation of the hand. Five phantoms were built with 0, 1, 20, 50 and 100 mg of added aluminum respectively. Regarding the anatomical simulation of flat, open hand, it was approximated with rectangle and bone is assumed to be evenly distributed throughout the whole hand. The hand dimensions are again put toward the upper limit of the typical range of the hand size.

Construction of this set of phantoms is supported by preliminary measurements of low concentration of aluminum phantoms (see Sec. 4.2). Thinner, rectangular geometry influenced process of aluminum activation and measurement in three different ways. One, it reduced neutron absorption in the rest of added atoms, lowering the screening effect on aluminum, and therefore, allowed better activation of all aluminum present in the phantom. Second, this geometry also reduced gamma rays attenuation inside the phantoms itself increasing the gamma signal acquired by the detectors. The third effect of thinner geometry made it feasible to move the two, large surface areas NaI(Tl) detectors closer (4.5 cm compared with 9 cm for cylindrical phantom), approaching 4π-geometry and increasing solid angle.

Chapter V

Calibration Curves and Minimum Detectable Limits

5.1 Data For The Initial, Cylindrical Set of Phantoms

5.1.1 Data Acquired using Two NaI(Tl) Detectors

Once the research on the system design and characterization of the neutron source was completed, initial work on aluminum activation was begun using cylindrical phantoms. Three minutes of exposure to a neutron beam was followed by a 20-30 s transfer time, and the γ-ray spectrum was then acquired for 5 minutes using two large thallium doped sodium iodide detectors (200 x 50 mm thick) separated by 9 cm. The detectors were arranged in a quasi-4π geometry, built in a Pb-shielded environment (see Sec. 3.1 and 3.2 for more details).The activation of phantoms was at 42 cm from the Li-target, aligned along the beam axis. During this experiment, the reading on a neutron monitor inside the target room was 14 mSv/h.

Each phantom was measured three times, and the peak amplitude of aluminum and calcium were determined using Marquardt analysis (Sec. 3.3). For each set of measurements the mean Chi squared value per degree of freedom was within one standard deviation of unity, indicating that the fitting routine was appropriate.

The calibration curve was obtained by plotting the ratio of amplitudes (Al/Ca) versus aluminum concentration (Sec. 3.3.3), and the regression line for the cylindrical set of phantoms was as follows

$$Al / Ca = (0.39 \pm 0.02) + (0.017 \pm 0.001) Al$$

The minimum detection limit (MDL) was (13±2) mg of Al (Pejović-Milić A. et al, 1997). A significant positive intercept suggested that there is aluminum contamination in these phantoms of 9 mg per 37.52 g of ash (Palerme S., 1993). After correcting for aluminum impurities, the intercept and slope were found to be (0.24±0.02) counts and (0.017±0.001) counts/mg respectively. It may be seen that some aluminum contamination is present from other chemicals used.

It is interesting to point out that aluminum contamination in phantoms was estimated in two different ways; one using the NAA (9 mg per phantom), and the other using a mass spectroscopy (15.47 mg per phantom). A same order of magnitude of 23 mg may be estimated from previous equation taking the ratio of intercept to slope.

To explore different parameters for the irradiation procedure the same phantoms were activated at 6 cm from the target. This modification considerably increased the number of neutrons that interacted with the phantom. Furthermore, it permitted the neutron field in the target room to be lowered while maintaining satisfactory activation of the aluminum. The neutron field at standard position was 5.5 mSv/h. Table 5.1 and graph 5.1 comprise the results of these measurements, after all necessary corrections on Al and Ca peaks amplitudes were done.

Al mass (mg)	Al/Ca ratio		
0	1.011±0.021	0.951±0.020	0.998±0.019
0.5	0.990±0.020	0.972±0.022	1.030±0.019
2	0.964±0.028	1.023±0.025	0.998±0.030
5	1.161±0.043	1.186±0.045	1.157±0.043
20	1.661±0.057	1.640±0.055	1.680±0.053
50	2.500±0.060	2.561±0.065	2.554±0.068
Calibration line	Al/Ca = (0.980±0.04) + (0.031±0.002) Al		
Corrected calibration line	Al/Ca* = (0.49±0.05) + (0.031±0.002) Al*		

Table 5.1 Al/Ca ratio and calibration curves for the cylindrical set of phantoms measured using two NaI(Tl) detectors; Irradiated at 6 cm from the target.

The distance of 6 cm was chosen rather than a shorter one because of the rapid divergence of the neutron beam. Although the neutron flux will increase as the distance between the phantom and the target decreases, according to the inverse square law the beam is too narrow to irradiate the whole phantom placed closer. Also, this distance allows enough space for easy placement of the polyethylene cavity.

Again the calibration curve shows the presence of aluminum contamination (figure 5.1). Correcting for the estimated quantity of aluminum (15.47 mg per phantom) by mass spectrometry (see Sec 4.3) led to an improved curve, but some impurities still remain undiscovered, since the intercept of the calibration line is above zero and not within uncertainty of zero.

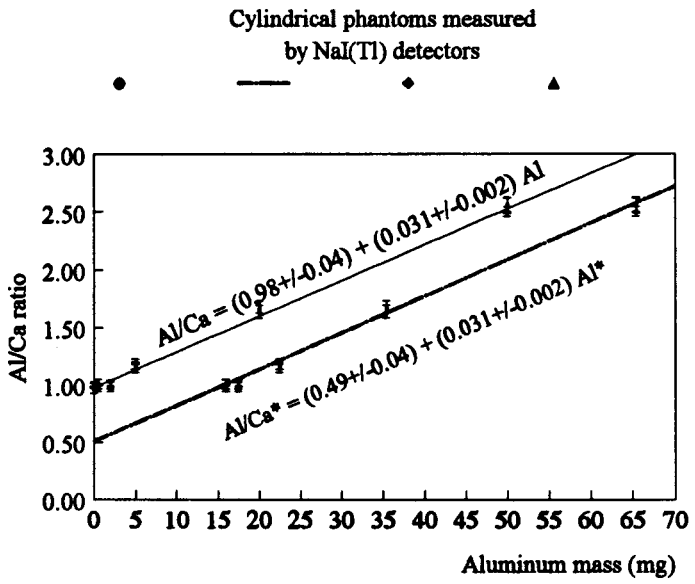

Figure 5.1 Variation of the ratio of the fitted peak amplitudes for the Al and Ca peaks for the cylindrical set of phantoms with aluminum content, measured using two NaI(Tl) detectors; Irradiation at 6 cm from the target.

Measurements give a minimum detectable limit of 1.3 mg in the hand which is above the normal concentration of aluminum in the hand of 0.4 mg. Since the Al/Ca ratios for the 0 and 0.5 mg phantoms are hardly distinguishable, the uncertainty of both phantoms were averaged to give 0.020, and this value was used to calculate the MDL rather than only the averaged uncertainty in the 0 mg phantom.

Although the same experiment procedure was used for irradiation at 6 cm as for previous measurement at 42 cm, the slopes of these two calibration lines differ from each other. It was expected, since the preliminary measurements at 42 cm were done using only the polyethylene moderator. The irradiation cavity was optimized and built after these promising results, and used throughout further experiments (see Sec. 2.2 and 2.3).

5.1.2 Data Acquired using a HPGe Detector

The possibility of using high resolution germanium detectors, as opposite to NaI(Tl), was examined (Sec 3.2.2). Keeping the same irradiation parameters such as the irradiation time of 3 minutes and the neutron field of 5.5 mSv/h, the distance to the target was decreased to 2.5 cm. During data acquisition, the phantoms were placed to touch the surface of a single HPGe detector, and further, detection limits were calculated for this setup.

Table 5.2 lists the results and calibration curves obtained by a linear regression over all experimental points.

Al mass (mg)	Al/Ca ratio		
0	1.021±0.036	1.039±0.035	1.102±0.037
0.5	1.210±0.047	1.180±0.043	1.233±0.040
2	0.907±0.031	1.235±0.057	1.022±0.033
5	1.340±0.042	1.454±0.044	1.267±0.055
20	2.118±0.066	2.071±0.065	2.194±0.068
Calibration line	Al/Ca = (1.1±0.1) + (0.052±0.004) Al		
Corrected calibration line	Al/Ca* = (0.25±0.12) + (0.052±0.004) Al*		

Table 5.2 Al/Ca ratio and calibration curves for the cylindrical set of phantoms measured using a HPGe detector; Irradiated at 2.5 cm from the target.

Based on these measurements the same minimum detectable limit of 1.3 mg was calculated as for data acquired by NaI(Tl) detectors. In this case the average uncertainty in the 0 mg phantom of 0.035 was used to calculate the MDL since the Al/Ca ratios for 0 and 0.5 mg phantoms are well distinguishable.

It is interesting to note that the same minimum detectable limit has been obtained with two different detection systems. Closer investigation shows that the NaI(Tl) detectors give more accurate measurements since the error on the Al/Ca ratio for phantoms with small aluminum mass is less than the error on the Al/Ca ratio measured using the HPGe detector for the same phantom. Further, due to change in the detection system and fitting routine the calibration slopes differ, but coincidentally the MDL remains the same.

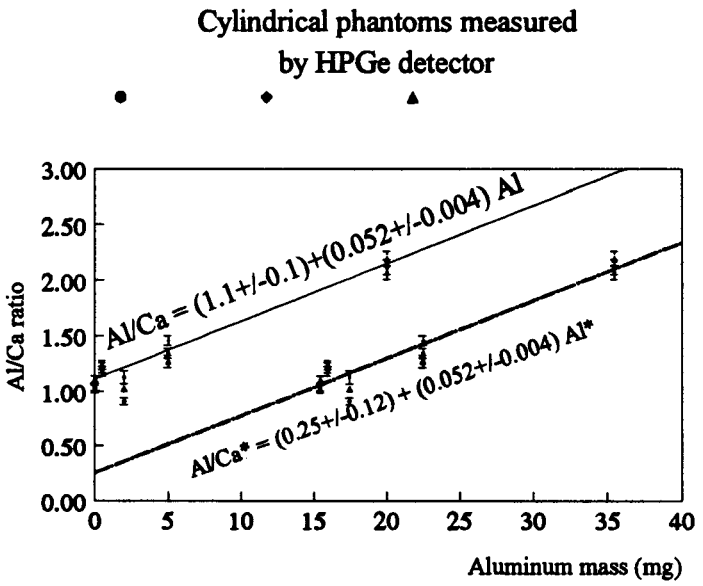

Figure 5.2 Variation of the ratio of the fitted peak amplitudes for the Al and Ca peaks for the cylindrical set of phantoms with aluminum content, measured using a HPGe detector; Irradiated at 2.5 cm from the target.

Assuming the same characteristics and minimum detectable limit for the set of HPGe detectors, to measure 0.3-0.4 mg of aluminum in a normal hand the detection system would need to be composed of as many as 19 HPGe detectors organized in a 4π-geometry. This number of detectors clearly eliminates the use of HPGe detectors for the aluminum

measurement in the hand. One reason is that an assembly of HPGe, usually has different sizes and performance characteristics, and thus do not significantly improve the detection system. On the other hand, this assembly would be too expensive. Also, the superior resolution of germanium detector is not crucial for this experiment, but the efficiency of an adequate detection system is. It is a well known fact that NaI(Tl) detectors are more efficient than the HPGe (Knoll G.F, 1989; Green S and Chettle D.R., 1992). Therefore, the NaI(Tl) setup would make a more effective detection system.

A request for a lower detectable limit has led to a different approach such as change in the phantom size and shape.

5.2 Data For The New, Flat Set of Phantoms

5.2.1 Data Acquired using Two NaI(Tl) Detectors

To investigate the possibility of improving the system design and lowering the detection limit, a set of flat phantoms simulating an open hand, doped with low concentrations of aluminum was made using the same chemicals as for the cylindrical ones (Sec. 4.2). In this preliminary work, the same slope of the calibration curve and aluminum contamination as found for the cylindrical phantoms were assumed (Sec. 5.1.1). The detection limit was estimated to be (2.5±0.4) mg Al (Pejović-Milić A. et al, 1997). Also, the acquired spectra of the flat phantoms have a ^{24}Na summed peak at 4.1 MeV, which had not been previously seen, clearly showing the improved detection efficiency (figure 3.2).

Based on this experiment a second set of flat phantoms was built, but with different bone simulation chemicals (see Sec. 4.4) to decrease the aluminum contamination.

Al mass (mg)	Al/Ca ratio		
0	0.519± 0.011	0.559±0.010	0.500±0.014
1	0.650±0.010	0.599±0.011	0.647±0.012
20	1.384±0.027	1.401±0.025	1.391±0.027
50	2.342±0.045	2.389±0.048	2.297±0.046
100	3.537±0.069	3.588±0.071	3.514±0.064
Calibration line	Al/Ca = (0.66±0.14) + (0.03±0.01) Al		
Corrected calibration line	Al/Ca* = (0.60±0.14) + (0.03±0.01) Al*		

Table 5.3 Al/Ca ratio and calibration curves for the flat set of phantoms measured using two NaI(Tl) detectors; Irradiated at 6 cm from the target.

Using the standard experimental procedure for phantom activation, the flat phantoms ranging from 0 to 100 mg were activated and, after all required correction, Al/Ca ratios were calculated (table 5.3).

The calibration curve, and corrected calibration curve for aluminum contamination in new phantoms (1.87 mg per phantom, Sec 4.3, table 4.2), over all experimental points are plotted on figure 5.3.

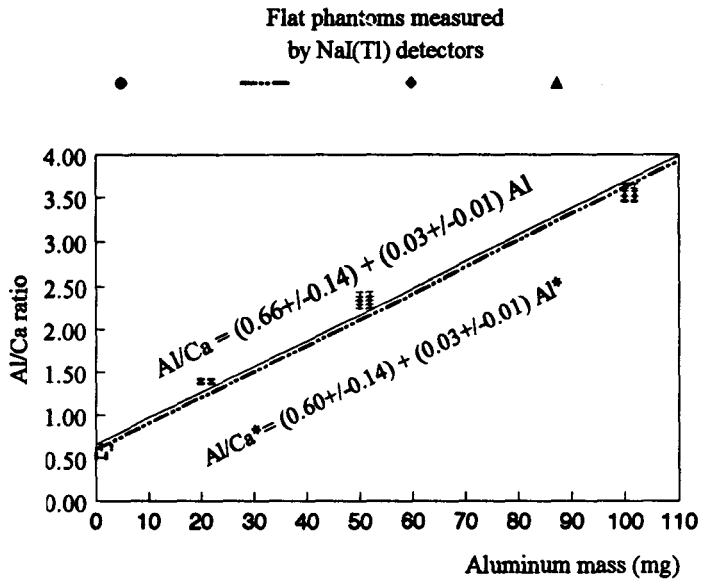

Figure 5.3 Variation of the ratio of the fitted peak amplitudes for the Al and Ca peaks for the flat set of phantoms with aluminum content measured used two NaI(Tl) detectors; Irradiated at 6 cm from the target.

A much enhanced minimum detectable limit of 0.7 mg has been obtained with the flat phantoms. An average uncertainty for the 0 and 1 mg phantoms equal to 0.011 was introduced in common definition of lower limit of detection. Unfortunately aluminum contamination still exists, as can be seen by the intercept of the calibration line of (0.60±0.14)

counts. Although a mass spectrometry technique was employed to measure a low quantity of aluminum in used chemicals, there is remaining aluminum. The source of contamination might be in other chemicals than calcium phosphate and resin which have been analyzed. Since all chemicals used to build new phantoms were of high purity, this might indicate a good sensitivity of procedure. Also, the intercept is the same as the predicted MDL within uncertainty, and therefore it is unrealistic to expect to be able to measure any lower aluminum concentration even if pure chemicals were used.

The slope of the calibration line may be used as a characteristic of overall properties set during the procedure such as irradiation parameters and geometry, counting system and its geometry, and fitting routing. Comparing the slopes of the calibration curves obtained for both cylindrical ((0.031±0.002)counts/mg) and flat ((0.03±0.01)counts/mg) phantoms, it is interesting to note that slopes do not differ from each other within uncertainty. This shows that aluminum measurement accomplished with the two sets of phantoms was repeated in the same fashion.

5.2.2 Data Acquired using HPGe Detector

Flat phantoms were not measured using the HPGe detector. A size difference between the phantom and the detector's surface led to the conclusion that the loss of a radiation would be significant for a precise measurement. Also, results presented in section 5.1.2 support no demand for these measurements.

5.3 An Accelerator Based *In Vivo* Measurement of Aluminum in Human Bone by Neutron Activation Analysis

The overall performance in terms of minimum detectable limit (MDL) and hand dose achieved, for both sets of phantoms and two detection systems, are summarized in tables 5.4 and 5.5. Assuming that 1.5 % of total body skeleton and skin is in one hand, and that 0.1 % of the hand dose will be delivered to the rest of the body, the effective doses have been calculated and included in the tables.

Cylindrical phantoms	MDL (mg)	Hand dose (mSv)	Effective dose* (μSv)	MDL x √ Hand dose
NaI(Tl) at 42 cm	13	2	2.6	18.4
HPGe at 2.5 cm	1.3	9	11.7	3.6
NaI(Tl) at 6 cm	1.3	6	7.8	3.2

* Assuming that 1.5 % of total body skeleton and skin is in one hand, and that 0.1 % of the hand dose will be delivered to the rest of the body;

Table 5.4 Performance of different detectors (MDLs) and doses delivered to the cylindrical set of phantoms during the aluminum measurement.

Flat phantoms	MDL (mg)	Hand dose (mSv)	Effective dose* (μSv)	MDL x √ Hand dose
NaI(Tl) at 42 cm	2.5**	2	2.6	3.5
HPGe at 2.5 cm	N/A	9	11.7	N/A
NaI(Tl) at 6 cm	0.7	6	7.8	1.7

* Assuming that 1.5 % of total body skeleton and skin is in one hand, and that 0.1 % of the hand dose will be delivered to the rest of the body;
** Estimated MDL value;

Table 5.5 Performance of different detectors (MDLs) and doses delivered to the flat set of phantoms during the aluminum measurement.

The results accomplished in this work show improvement in terms of MDL, and the best result being an MDL of 0.7 mg with a 6 mSv dose equivalent delivered to the hand. This MDL is comparable to the Brookhaven measurements (Sec. 1.3, table 1.1), but the delivered hand dose, which is the upper limit estimate for the equivalent dose, is one order of magnitude lower than the results from other groups.

It must be emphasized that the neutron dose monitor was a Snoopy, which uses an average quality factor to convert the dose readings to a dose equivalent rate. The average values depends on the field in which the monitor has been calibrated. Thus, for the hand dose reported in this study, the quality factors used in the monitor was based on ICRP 26. On the other hand, the dose equivalent to the hand may be independently calculated from a flux measurement using indium foils (Sec. 2.2), and applying the fluence to dose equivalent conversion factors. For thermal neutrons, a fluence of 26 $n/cm^2/s$ converts to a dose equivalent of 1 μSv/h (ICRP 21, 1971). For the average neutron flux measured inside the irradiation cavity at 2.5 and 42 cm from the target, and for 3 minute irradiation, the dose equivalent to the hand would be 6 and 0.2 mSv respectively. This dose equivalents are considerable smaller than the hand doses of 9 and 2 mSv measured by the Snoopy. This may imply that the Snoopy's dose is an overestimation. Furthermore, the dose equivalent estimated from the activation foils does not take into consideration the presence of a small resonance component nor the moderate/fast neutron component and gamma rays. Thus, this is offered as a lower limit of the actual hand dose equivalent. Choosing a conservative approach rather than underestimating the delivered dose, the higher dose equivalents measured by the neutron

monitor are reported in this study. Microdosimetry may solve this dilemma, and may determine a lower dose equivalent than presented in tables 5.4 and 5.5, further decreasing the (MDL x √hand dose) value.

The MDL is influenced by change in the irradiation settings. If the dose were to be increased by a factor of 3, the MDL obtained for flat phantoms measured by NaI(Tl) detectors would decrease by approximately the square root of 3, which would make it the same as the expected aluminum level in the normal hand (0.4 mg). The dose may be increased in different ways such as increase the irradiation time, incident proton current or neutron flux. This increase in the dose delivered to the hand, although in contrast with the ALARA principle, would be well below the annual background exposure to radiation since the effective dose would be of the order of 1 % of annual background. Also, the MDL decreases as the counting time increases. Unfortunately there is a limitation due to the short half life of ^{28}Al, therefore, there is no reason to measure aluminum longer than 600 s. This doubled counting period may lower the MDL to 0.5 mg. If both parameters were simultaneously changed the resulting MDL would be 0.3 mg.

The other possibility for decreasing the MDL is to lower an incident proton energy. Empirically it has been measured if the proton energy is 2.05 MeV to keep the same dose, the current must be increased by roughly a factor of 5 that will increase the thermal neutron flux by approximately 2. This would result in a decrease in the MDL by the square root of 2 giving the MDL of 0.5 mg. The greatest improvement in the MDL with the least effect on the delivered dose may be achieved by maintaining the same proton energy, but simultaneously increasing the current and decreasing the irradiation time. For the irradiation of 60 s with

increase in the current by factor of 3 (~ 75 μA) the net MDL would be 0.61 mg with the unchanged hand dose. Also, maintaining the same dose but drastically increasing the current by factor of 20 (~ 500 μA) and decreasing the irradiation time by the factor of 6 (30 s) may give the MDL as low as 0.41 mg that is the expected aluminum concentration in a healthy subject's hand.

It is useful to mention that the physiologically realistic quantities of calcium in both sets of phantoms enabled the ratio Al/Ca to be established, which is an important parameter for actual patients measurements because it allows determination of aluminum level per gram of calcium. This eliminates the dependence of measurements on the hand size, possible movements as well as the irradiation and counting geometry.

The presented results are very encouraging, and suggest that the use of an accelerator based neutron activation system could be used for the direct *in vivo* monitoring of bone aluminum values in patients, providing an alternative choice to painful bone biopsy, for the detection of aluminum intoxication from long-term exposure.

5.4 Future Development of an Accelerator Based *In Vivo* Aluminum Measurement in Bone

Regarding possible *in vivo* experiments, the procedure as described is more sensitive to detect the low level of aluminum found in normal subjects than previously published, but it is still not sufficiently sensitive to detect as low as 0.3 to 0.4 mg of aluminum in the hand of healthy subject. However, the developed procedure is a suitable means of screening patients with significantly elevated levels, which can be up to 50 times normal, as found in patients with renal failure (Ellis K.J. et al, 1988; Wyatt R.M. et al, 1993).

One approach to investigate the possible use of this procedure is to compare measurements with the results measured using an atomic absorption spectrometry in iliac crest bone biopsy specimens. Other ways to test the procedure might be parallel chemical or X ray spectroscopy analysis of pathological bone samples. Studying pathological bone samples may simultaneously give an answer about a different aluminum deposition in cortical versus trabecular bone, and the homogeneity of aluminum deposition in the skeleton. Throughout all previous publications and for this work the homogeneity of aluminum storage in skeleton have been assumed.

To build a more precise and accurate system some modifications have to be done. One may be to improved the moderator / shielding assemble. Any carbon hydrate, such as wax or

polyethylene, may be used around the beam line and target to proposed patient position from neutrons emitted in directions from 90° to 180°. Furthermore, a reflector behind the irradiation cavity might be added to increase the neutron flux inside the cavity, and to reduce radiation damage to the rest of the body (Green S. and Chettle D.R., 1992).

Possible moderating material has to have a low macroscopic absorption cross section, Σ_{abs}, while having a high value for the average energy loss per collision, ξ. Polyethylene, water, heavy water and graphite are materials typically used to slow down fast / moderate neutrons to thermal. Water as a moderator provides the additional advantage that it surrounds the hand and, has similar moderating properties to tissues, eliminates the need to correct for tissue thickness (Wyatt R.M. et al, 1993). Some preliminary simulations were done to calculate difference in the neutron thermal flux placing polyethylene, graphite or heavy water as moderator using Monte Carlo Neutron and Photon (MCNP) software produced by Los Alamos. A simple experimental geometry was simulated with an isotropic source in the center of twelve concentric spheres. A 5 cm sphere of air surrounded the source with remaining spheres 2 cm apart and containing the material of interest. Software was run over 1,000,000 particles for high precision. The relative thermal neutron flux (neutrons per cm^2) for each surface was calculated.

Material	water	graphite	heavy water
Density (g/cm^3)	1	1.65	1.1
Macroscopic scattering cross section (cm^{-1})	1.613	0.398	0.353
Macroscopic absorption cross section (cm^{-1})	0.022	3.7×10^{-4}	8.5×10^{-5}

Table 5.6 Relevant data to calculate the neutron flux using possible materials as moderators.

To measure aluminum in human bone a high flux of thermal neutrons is essential, which implies that polyethylene is the best moderator (see figure 5.4). The calculated thermal flux with polyethylene as a moderator is five times greater than for graphite or heavy water. The decrease of the flux with increased thickness of polyethylene is more rapid than for the other two materials, which may be explained by the fact that polyethylene has an absorption coefficient greater than that of graphite or heavy water (table 5.6).

For further understanding of the presented results some relevant data are shown in table 5.7. As may be seen, that the mean free path of thermal neutrons in water, which has similar properties as polyethylene, is lower than in graphite or heavy water. A difference may be seen in the energy loss and the number of collisions necessary to slow 520 keV neutrons to 0.025 eV as well. As expected, the average energy loss is the smallest for graphite, because of the mass difference between carbon and a neutron. Graphite thus requires the greatest number of collisions to slow neutrons from

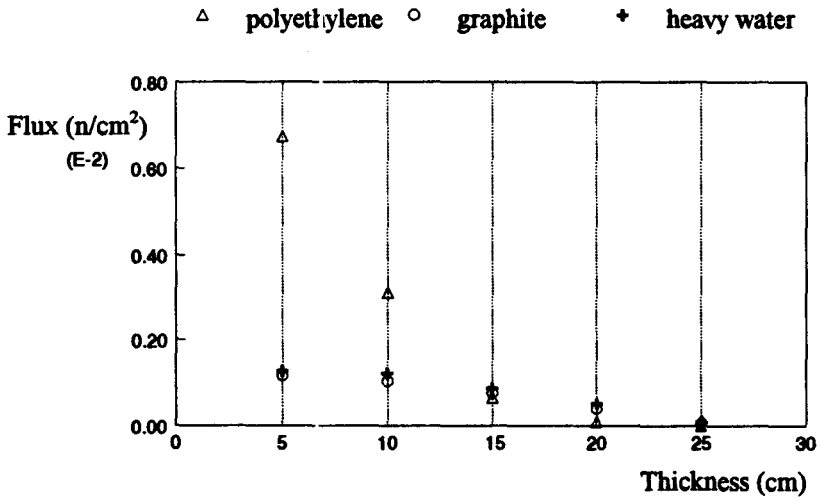

Figure 5.4 MCNP simulation for possible moderator materials.

520 keV to thermal region. A large values for ξ, means fewer collisions needed to slow down the neutrons. This does not consider the scattering cross section. If a moderator has a small scattering cross section then this material may be less advantageous that one with a big probability to scatter and a smaller ξ. A moderation ratio takes into consideration both macroscopic cross sections and average energy loss.

Material	water	graphite	heavy water
Mean free path (cm)*	0.61	2.51	2.83
Energy loss ξ*	0.93	0.158	0.51
Number of collisions to slow neutrons from 520 keV to 0.025 eV	7.87	46.32	14.35
Moderating ratio (Σscatt x ξ / Σabs)	69	170	2100

* (Valente F.A., 1963)

Table 5.7 Properties of some moderators.

The best material to use for a moderator should be heavy water, however, the moderator usually used is graphite since it is easier to handle. These results support the use of a polyethylene cavity, beside its handiness, but not exclude further design change by adding a reflector, likely graphite. Polyethylene provides a good shielding material because of its ability to absorb neutrons. More neutron transport simulations have to be done prior to a decision about which moderator/shielding design will best improve the sensitivity of the system.

A cyclic activation technique (Wyatt R.M. et al, 1993) may be the solution for potential patient measurement in order to increase 1.78 MeV gamma-ray activity. Some phantom measurements have been done, but it still has to be investigated how the sensitivity

of the procedure can best be improved, e.g. delivering a higher dose, further optimization of the irradiation cavity or by changing the irradiation settings.

Prior to any *in vivo* measurement a more accurate dose measurement must be performed. A dose delivered to the hand is intimately associated with the optimum incident proton energy, beside the shortest possible irradiation time and irradiation cavity design. The use of microdosimetric counters may give detailed information about the neutron dose which is distributed among recoil particles with different ionization densities, and also provide a precise measurement of absorbed dose. The neutron microdosimetry will lead to a choice of optimum proton energy for aluminum activation since it measures deposited energy, linear energy density and, hence, the quality factor. Determination of the beam quality for each proton energy will show the variation of aluminum sensitivity with proton energy and thus, with neutron energy. This could result in the calculation of physical and biological relevant dose, without an employment of nominal quality factor.

Once these adoptions have been completed they would open a broad field of *in vivo* measurements of aluminum in human tissue. The boundaries of future *in vivo* research may not be seen yet since our knowledge about aluminum, its metabolism and possible health effects, is finite.

REFERENCES AND BIBLIOGRAPHY

Alfrey A.C et al, 1976. The dialysis encephalopathy syndrome: Possible aluminum intoxication, *N Engl J Med*, **294**, pp.184-188.

Alfrey A.C, 1984. Aluminum intoxication, *N Engl J Med*, **310**, pp.1113-1115.

Bevington P.R., 1992. Data Reduction and Error Analysis for the Physical Sciences, Second Edition, McGraw-Hill, Inc., New York, pp.161.

Bogdanovich E. et al, 1992. Non-Invasive Bone Aluminum Assay by Neutron Activation Analysis, *J Radioanal Nucl Chem*, letters **164 (5)**, pp. 293-302.

Chettle D.R., Fremlin J.H., 1984. Techniques of *in vivo* neutron activation analysis, *Phys Med Biol*, **29 (9)**, pp.1011-1043.

Cohn S.H., 1980. The present state of in vivo neutron activation analysis in clinical diagnosis and therapy, *Atom Energy Rev*, **18**, pp. 599.

Crapper D.R. et al, 1980. Intranuclear Aluminum Content in Alzheimer's Disease, Dialysis Encephalopathy, and Experimental Aluminum Encephalopathy, *Acta Neuropathol*, **50**, pp.19-24.

Dahl E. et al, 1990. The early effects of aluminum deposition and dialysis on bone in chronical renal failure: A cross-sectional Bone-Histomorphometric study, *Nephrol Dial Tranplant*, **5**, pp. 449-456.

Eastwood J.B. et al, 1990. Aluminum deposition in bone after contamination of drinking water supply, *The Lancet* August 25, pp. 462-464.

Ellis K.J. et al., 1988. In vivo monitoring of skeletal aluminum burden in patients with renal failure, *Journal of Radianalytical and Nuclear Chemistry, Articles,* **124 (1)**, pp. 85-95.

Green S. and Chettle D.R., 1992. A feasibility study of the *in vivo* measurement of aluminum in peripheral bone, *Phys Med Biol,* **37 (12)**, pp. 2287-2296.

Green S. et al, 1993. Characteristics of an accelerator based system for *in vivo* aluminum measurement in peripheral bone, *Human Body Composition*, Edited by K.J. Ellis and J.D. Eastman, Plenum Press, New York, pp. 289-293.

ICRP, 1971. Data for the protection against ionizing radiation from external sources, No. **21**, Pergamon Press, Oxford, pp.52-53.

ICRP, 1975. Report of the task group on Reference Man, No. **23**, Pergamon Press, Oxford.

ICRP, 1977. Recommendation of the ICRP; Annals of the ICRP, No. **26**, Pergamon Press, Oxford.

ICRP, 1994. Basic Anatomical and physiological Data for use in Radiological Protection: The Skeleton, No. **70**, Pergamon Press, Oxford.

Lefebvre A. et al, 1988. Cortical *v* trabecular bone aluminum in dialyzed patients, *Am J Kidney Dis*, **12 (3)**, pp. 220-226.

Martyn C.N. et al, 1989. Geographical relation between Alzheimer's disease and aluminum in drinking water, *The Lancet* January 14, 1989, pp. 59-62.

McLachlan D.R.C et al, 1991. Would decreased aluminum ingestion reduce the incidence of Alzheimer's disease?, *Can Med Assoc J*, **145 (7)**, pp. 793-804.

Moreno A. et al, 1994. Aluminum in the neonate related to parenteral nutrition, *Acta Pediatr.*, **83**, pp.25-29.

Nicar M.J. et al, 1992. Brain and Bone aluminum: A Composition of Aluminum intake in Rats, *Envirom Toxico Chem*, **11**, pp.1331-1336.

O'Mahony D. et al, 1995. Bone Aluminum Content in Alzheimer's Disease, *Dementia*, **6**, pp.69-72.

Palerme S. et al, 1993. Pilot studies for *in vivo* bone aluminum measurements, *Human Body Composition*, Edited by K.J. Ellis and J.D. Eastman, Plenum Press, New York, pp. 303-306.

Palerme S., 1993. Pilot studies for *in vivo* bone aluminum measurements, A Master Thesis, McMaster University, Hamilton.

Pejovic-Milic A. et al, 1998. Development of an Accelerator Based Determination of Aluminum Burden in Peripheral bone by Neutron Activation Analysis, *Appl Radiat Isot*, in press.

Rainbow A. J., 1995. Biology 4U3/6U3 course handout, McMaster University, Hamilton.

Rifat S.L. et al, 1990. Effect of exposure of miners to aluminum powder, *The Lancet*, November 10, 1990, pp. 1162-1165.

Rodushkin I. et al, 1995. Aluminum in surface water of the Kola Peninsula, Russia, *The Science of the Total Envronment*, **163**, pp. 55-59.

Rogers D.W., 1979. Why not to trust a neutron remmeter, *Health Physics*, **37(6)**, pp.735-742.

Schmid K. et al, 1995. Use of bone mineral content determination by X-ray absorptiometry in the evaluation of osteodystrophy among workers exposed to aluminum powders, *The Science of the Total Envronment*, **163** , pp. 147-151.

Scott M.C. and Chettle D.R., 1986. In vivo elemental analysis in occupational medicine, Reviews, *Scand J Work Environ Health*, **12**, pp. 81-96.

Valente F.A., 1963. A manual of experiments in reactor physics, edit by the Macmillan Company, New York, pp. 321.

Wills M.R. and Savory J., 1983. Aluminum poisoning: Dialysis encephalopathy, osteomalacia, and anemia, *The Lancet*, July 2, 1983, pp. 29-33.

Worth D.P. et al, 1989. Quantitative Bone Scanning in the Diagnosis of Aluminum Osteomalacia, *Nephrol Dial Transplant*, **4**, pp.721-724.

Wyatt R. M. et al., 1993. The development of a technique to measure bone aluminum content using neutron activation analysis, *Physiol Meas*, **14** , pp. 327-335.

Wyatt R.M. et al., 1993. Development of an *in vivo* neutron activation analysis technique to measure bone aluminum, *Human Body Composition*, Edited by K.J. Ellis and J.D. Eastman, Plenum Press, New York, pp. 319-321.

Yanch J.C. et al, 1992. Accelerator-based epithermal neutron beam design for neutron capture therapy, *Med Phys*, **19 (3)**, pp.709-721.